UNIVERSITÀ DEGLI STUDI DI MILANO BICOCCA

Ph.D. Program
Translational and Molecular Medicine

Rational design of targeted therapies for Pancreatic adenocarcinoma in K-ras GEMMs

Coordinator: Prof. Andrea Biondi

Tutor: Prof. Andrea Biondi

Dr. Gianmarco Contino

Matr. No. **760756**

XXVII CYCLE

ACADEMIC YEAR

2013-2014

Table of Contents

Abstract

Pancreatic ductal adenocarcinoma (PDAC) is one of the deadliest cancers in western countries, with a median survival of 6 months and an extremely low percentage of long-term surviving patients. KRAS mutations are known to be a driver event of PDAC, but targeting mutant KRAS has proved challenging. As new targeted agents are becoming available for clinical trial we aimed to design improved therapeutic approaches for the treatment of pancreatic ductal adenocarcinoma by means of in vitro and in vivo models of pancreatic adenocarcinoma.

Methods We analyzed the results of a high-throughput screening of >500 human cancer cell lines (including 46 PDAC lines), for sensitivity to 50 clinically-relevant compounds. We designed two different strategies including 1) a JAK2 inhibitor that blocks STAT3 function and 2) a MEK1/2 inhibitor, AZD-6244, for efficacy alone or in combination with the PI3K inhibitors, BKM-120 or GDC-0941, in a KRASG12D-driven GEMM that recapitulates the multi-step pathogenesis of human PDAC.

Results 1) JAK2 inhibitor: Large-scale screening of cancer cell lines with a JAK2 inhibitor that blocks STAT3 function revealed a >30-fold range in sensitivity in PDAC, and showed a close correlation of sensitivity with levels of tyrosine-phosphorylated STAT3 and of the gp130 receptor, an upstream signaling component. Correspondingly, upregulation of the IL6/LIF-gp130 pathway accounted for the strong STAT3 activation in PDAC subsets. To define functions of STAT3 in vivo, we developed mouse models that test the impact of conditional inactivation of STAT3 in KRAS-driven PDAC. We showed that STAT3 is required for the development of the earliest pre-malignant pancreatic lesions, acinar-to-ductal metaplasia (ADM) and pancreatic intraepithelial neoplasia (PanIN). Moreover, acute STAT3 inactivation blocked PDAC initiation in a second in vivo model. Our results demonstrate that STAT3 has critical roles throughout the course of PDAC pathogenesis, supporting the development of therapeutic approaches targeting this pathway. Moreover, our work suggests that gp130 and phospho-STAT3 expression may be effective biomarkers for predicting response to JAK2 inhibitors. **2) MEK1/2/PI3K inhibitors**: In vitro screens revealed that PDAC cell lines are relatively resistant to single-agent therapies. The response profile to the MEK1/2 inhibitor, AZD-6244, was an outlier, showing the highest selective efficacy in PDAC. While MEK inhibition alone was mainly cytostatic, apoptosis was induced when combined with

PI3K inhibitors (BKM-120 or GDC-0941). When tested in a PDAC GEMM and compared to the single agents or vehicle controls, the combination delayed tumor formation in the setting of prevention and extended survival when used to treat advanced tumors, although no durable responses were observed.

Conclusions: Our studies point to 1)JAK2 as a therapeutic target in GP130 high pancreatic cancers and 2) important contributions of MEK and PI3K signaling to PDAC pathogenesis suggesting that dual targeting of these pathways may provide benefit in some PDAC patients.

Chapter 1. General Introduction

Clinical problem

Pancreatic Cancer is the fourth leading cause of cancer death in the US with over 46,000 estimated new cases in 2014 in US only (source SEER, NCI). Disappointingly in the same year almost 40,000 patients will die of this cancer in the same year, as 5-year survival is extremely low: 5.4% (source SEER, NCI). Despite progresses in diagnostic and therapeutics we were only able to improve this figure of 2.4% in over 40 years, an appalling comparison with other malignancies. Causes of failure are certainly in the late diagnosis, the anatomical location and peculiar parenchymal composition of the pancreas, which makes surgical procedure extremely unforgiving and prone to poor results, and the exceedingly abundant stromal component of the cancer, a difficult microenvironment that contributes to resistance and facilitate progression.

Genomics and Genetics of Pancreatic Adenocarcinoma

Inherited susceptibility to Pancreatic Cancer

Inherited predisposition to PDAC account for about 10% of cases and the first-degree relatives of PDAC patients have an increased risk of developing pancreatic and liver carcinoma (1.88- and 2.7-fold,

respectively); the risk it is nearly 3-fold higher when the proband is less than 60 years old at diagnosis.

Several familial cancer syndromes increase the risk of pancreatic cancer such as hereditary nonpolyposis colon cancer syndrome, hereditary breast-ovarian cancer syndrome (BRCA1 and BRCA2 genes), Peutz-Jeghers syndrome (LKB1 gene), familial atypical multiple mole melanoma syndrome (CDKN2A gene), von Hippe-Lindau syndrome (VHL), and ataxia-telangiectasia ATM gene (Al-Sukhni, 2008). The penetrance of PDAC in these kindreds is quite low (<10%), reflecting a role of progression rather than initiation of pancreatic premaligant lesions. Differently, families with hereditary pancreatitis, a syndrome characterized by recurrent pancreatitis and associated with germline mutations in PRSS1 and SPINK1, have a lifetime risk of 40% (by the age of 70) to develop PDAC, pointing out the tumorigenic role of chronic inflammation in PDAC initiation (Lowenfels, 1997). A striking additive effect is noted in smokers with hereditary pancreatitis who develop pancreatic cancer 20 years before non-smokers (Lowenfels, 2001). A rare mutation occurring in the PNCA1 gene encoding for Palladin has been found in PDAC families linked to chromosome 4q32.3 (Pogue-Geile, 2006). Recently, truncating mutations in PALB2 gene were found in patients with late onset familial pancreatic cancer through an exomic

sequencing approach (Jones 2009). Although PALB2 mutations account less than 3% of familial pancreatic cancer, the finding corroborate a role for BRCA2 (a PALB2 binding partner) and BRCA2 related pathways particularly in progression of advanced lesions (Tischowitz et al, 2009 and Slater et al, 2010). In facts, impairment of the BRAC2 homologous-recombination DNA repair process might contribute to tumor progression favoring mutation after DNA-damage response pathways such INK4A or p53 are inactivated. Family registries are playing a fundamental role in identifying new mutations trough next generation sequencing and enrolling high-risk population in prospective follow-up and screening studies (reviewed by Kelin, 2013)

Genetics susceptibility to sporadic Pancreatic Adenocarcinoma

A multicentric effort to elucidate genetic contribution to sporadic pancreatic cancer has been recently undertaken in GWAS by the use of a high density Single Nulceotide Polymorfisms (SNPs) platform (Illumina) (Amundadottir et al., Nature Genet, 2009; Petersen et al., Nature genet, 2010). Authors collected a total of 3,851 cases and 3,943 controls from 12 different prospective cohorts and 8 case-control studies and identified the AB0 locus (9q34.2) as a

susceptibility locus for pancreatic cancer. Three additional loci were identified (13q22.1, 1q32.1 and 5p15.33) by a second GWAS on 3990 samples from the same 8 case control studies and combined with the dataset from the previous studies. Intriguingly, association of AB0 blood group with GI cancers was reported in the 1950s and '60s and a recent report of the Pancreatic Cancer Cohort Consortium (Wolpin et al, 2010) confirmed that A and B groups yield an higher risk of developing pancreatic cancer (O.R. range: 1.36-2.42) when compared to O group in 12 prospective cohorts. Yet, from a biological standpoint, it is not clear how variations of the ABO gene encoding a glycosyltransferase that catalyzes the transfer of carbohydrates onto the H antigen to form the A, B or O antigen can confer a higher predisposition to pancreatic cancer. Circulating serum levels of TNFalpha, soluble intracellular adhesion molecule of sICAM-1 (soluble intracellular adhesion molecule), plasma levels of alkaline phosphatase, or differential expression of ABO in primary and metastatic tumors have also been claimed as possibly involved (Amundadottir et al., 2009). The 5p15.33 associated SNP fall in an intron of the CLPTM1L gene (encoding for cleft lip and palate transmembrane 1-like), that together with the adiacent TERT gene (encoding for telomerase reverse tanscriptase) is a locus associated also with bladder, prostate, lung and basal cell cancers and whose genes have been already implicated in

carcinogenesis. A common concern with GWAS is reproducibility in other dataset, but also the biases associated with rare variants and survivorship. In fact, highly lethal variants might be loss in case control studies especially for an aggressive cancer as pancreatic cancer. Despite they might provide some insight in genetic susceptibility to pancreatic cancer, GWAS contribution to the understanding of the biology of pancreatic cancer await confirmation by further study on the identified loci.

Major Genetic hits in PDAC initiation and Progression

Since the original description of an increased incidence of proliferative lesions in ducts and ductules adjacent to pancreatic adenocarcinoma (Cubilla and Fizgerald, 1976), an ordered progression of morphological alterations from early lesion (now denoted as PanINs of grade 1 to 3) to PDAC has been established and correlated with genetics events (Hruban et al., 2001). While the paradigm of ductal origin of PDAC has been recently questioned (see paragraph 5), the identification of this genetic hits has build a solid hierarchy of genes involved in progression and maintance of PDAC.

Activating KRAS mutations in codon 12 and less commonly in codon 13 or are an early event in about 30-87% of PDAC associated PanIN while in human PDAC, mutations can be found in 75-100% of cases and accumulates during progression (Almoguera et al., 1988, Rozenblum, 1997; Hruban et al., 1993, Jones 2009). KRAS activation is therefore an initiating step of PDAC tumorigenesis, but it is also required for maintenance of the tumor as suggested by various sources of evidences (Hirano et al, 2002; Fleming et al, 2005). As a proof of principle KRAS mutation allowed the development of successful animal models for pancreatic cancer. Intriguingly, KRAS is found mutated also in other alteration such as adenomatous hyperplasia, papillary hyperplasia, mucinous hypertrophy, and in squamous metaplasia (14-36%) and in PanIN lesions arising in the context of pancreatits (10%) (Lohr et al, 2005; Luttges et al, 2000; Feldman et al, 2006). In the search of a progenitor for PDAC Shi et al. (2009) utilized microdissecion to determine the mutational status of KRAS. Interestingly, Acinar Ductal Metaplasia(ADM) harbored KRAS2 mutations only in the context of PanIN, while isolated ADM foci did not. This may suggest that that PDAC may not arise from acinar cells and that PanIN associated ADM may instead represent a retrograde extension of the neoplastic PanIN (Shi et al, 2009). This search highlight the need of conclusive lineage tracking studies which are lacking at the moment.

Downstream targets of Ras signaling pathway can be occasionally interested by genetic events reflecting either mechanisms of redundancy or selection. B-RAF mutations are rare in PDAC but are present in 33% of pancreatic medullary carcinomas, an histologically distinct entity characterized by wild type KRAS and DNA mismatch repair defects (Calhoun, 2003; Ishimura, 2003). Amplification of AKT2, a downstream effector of PI3K, have been described in 10-20% of PDAC pointing out the potential relevance of the PI3K pathway for targeted inhibition.

An intriguing early genetic hit of PDAC, which characterize 80-95% moderately advanced lesions, is the loss of CDKN2A gene (Rozenblum, 1997). The CDKN2A (9p21) gene encodes two proteins that regulate critical cell cycle regulatory pathways, the p53 pathway and the retinoblastoma pathway. The mechanism involves shared coding regions and alternative reading frames through which CDKN2A gene produces p16(INK4A), an inhibitor of CDK4/6 meditated Rb phosphorylation, and p14(ARF), which binds the p53-stabilizing protein MDM2 but may possess additional p53 independent functions (Sharpless, 2005; Robertson and Jones, 1999). The target of CDKM2A loss is mainly INK4A, which occur in combination with ARF only in 40% of cases (Rozenblum, 1997). INK4A undergoes inactivation either because of homozygous deletion

(40%), homozygous deletion (40%) or promoter hypermethylation (Wilentz, 1998); this latter mechanism might be particularly important in PanIN where between 30-70% of lesions show loss of INK4A but homozygous deletion has been shown to occur in only 8% of cases (Wilentz et al, 1998; Hustinx et al, 2005).

The actual role of ARF might be reconsidered in view of the observation that CDKN2A and TP53 losses are not mutually exclusive in pancreatic cancer, as opposed to other tumors (Sharpless, 2005). However, it is possible that ARF loss play a major role in the impairment of tumor suppression upon DNA damage for which TP53 is dispensable (Cristophorou et al, 2006). As a matter of fact, TP53 is mutated in more than 50% of pancreatic adenocarcinomas (Rozenblum et al, 1997). TP53 loss in later-stage of dysplastic lesions is likely to contribute to the genetic instability that is a hallmark of pancreatic cancer (Aguirre et al, 2004; Hingorani et al, 2005; reviewed in Karhu et al, 2006). A mechanism of genetic instability of PDAC resides the biphasic behavior of telomere dynamics which favors initial telomere shortening and dysfunction, leading, in turns, to chromosomal rearrangement through breakage-fusion-bridge cycles, and lately reactivates telomerase to support cell survival (rev in Maser and De Pinho, 2002). This observation has been validated in a telomerase deficient mouse models where critically short

telomeres cooperate with TP53 loss to promote different tumors (Chin et al, 1999) and in a model of PDAC where chromosomal instability resulted as a signature effect of combined activated KRAS and a point mutation of TP53 ($Tp53^{R72H}$) (Hingorani et al, 2005). In human PDAC telomere dysfunction leads to the formation of anaphase bridges and extensive structural rearrangement of chromosome, triggering chromosomal fragmentation (Gisselsson, 2001). Telomere shortening is observed as early as in adenoma IPMN, a precursor of PDAC, and increases along progression to IPMN carcinomas and PDAC while high level telomerase activation occur at late stage of the disease (Suehara, 1997, Hashimoto 2008). Chromosomal and microsatellite instability are two other mechanisms that are likely to contribute to the genetic complexity of PDAC, as the higher incidence of PDAC in BRCA2 mutation carriers and HNPCC families might suggest (Breast Cancer Linkage cons, 1999; Lynch, 1985). The mechanisms underlying such tremendous aneuploidy and genomic heterogeneity within PDAC is likely to account for the resistance of this tumor to different chemo and radiotherapy regimens. However, it should be noted that this is also replicated at the level of single nucleotide variations where the number of diverse mutated genes is higher than other common cancers (Jones et al, 2009). In this context, the observation of a significant smaller amount of average of putative driver mutations in

PDAC when compared to colorectal and breast cancer may indicate the convergence of different carcinogenic mechanisms together which in turns need fewer divisions (Jones et al, 2009).

Accumulating cytogenetic and CGH studies have contributed in defining a map of common loci of amplification and deletion whose genomic alteration might contribute to carcinogenesis. This approach has been successful in the identification of the SMAD4/DPC4 gene, starting from the observation of the deletion of a genomic region on chromosome 18q21 in about 30% of PDAC. SMAD4 mutations or loss is a negative prognostic marker, involving 50% of PDAC and it should be considered a progression gene (Blackford, 2009; Wilentz 2000). This is supported by the evidence that SMAD4 loss only occur in late stage PanIN, and, when inherited as a germline mutation (as in juvenile polyposis syndrome), does not predispose to pancreatic cancer (Luttges et al, 2001; Heinmoller et al, 2000). SMAD4 is a target of TGFbeta signaling, a cytokine which, upon binding of TGFBRs, trigger the phosphorylation of cytoplasmic SMAD2 and SMAD3 to form a complex with SMAD4 and translocate into the nucleus to activate gene transcription. Mutations or deletions in the TGFbeta signaling can occasionally involve other members such as SMAD3 and more frequently TGFBR2 (Blackford et al, 2009). Inactivation of SMAD4 abolishes TGFbeta mediated tumor suppressive function but

maintains some tumor promoting TGFbeta responses in concert with RAS/Erk pathway, such as epithelial mesenchimal transition (EMT), which is required for cells to acquire a fibroblastic phenotype that promotes invasion and metastasis (Levy, 2005).

Structural Variants in PDAC

Cytogenetic, Spectra Karyotiping (SKY), and CGH have been extensively applied to PDAC primary tumors and cell lines Chromosomal abonormalities are present in nearly 100% PDAC cell lines and in 67-100% of primary tumors depending on contamination from normal cell component (Aguirre et al., 2004; Heidenblad et al., 2004; Holzman et al., 2004; Harada, 2002, Kitoh 2005, reviewed in Karhu 2005). A very high-level amplification has been detected at the 19q13.1–13.2 region within a three-megabase segment in the PANC-1 cell line. Several amplification events localized in known PDAC oncogene loci such as KRAS (at 12p12.1), MYC (8q24), and AKT2 (19q13) (Aguirre et al., 2004; Heidenblad, 2004). Intriguingly, amplification of 12p both proximal and distal to KRAS gene suggest that other players (among 20 putative target genes) might drive this genetic events in addition to the point mutation of the KRAS gene (Heidenblad et al., 2004). The dissection of the architecture of

disease associated loci challenges is likely to reveal a superior level of complexity in distant acting elements as suggested by the analysis of sequence polymorphisms associated with Coronary Artery Disease in a non coding region of the 9p21/CDKN2 locus cis-regulating the expression of *Cdkn2a* and *Cdkn2b*.

High troughput genome sequencing

Oncogenomics and trascriptome data have been fueled by the increasing availability of high throughput sequencing and analysis tools at way lower costs and pancreatic cancer is no exception. However the number and combination of different approaches, sample source and selection, and bioinformatic analysis account for the extreme heterogeneity of data available to date. Whole genome scans in search of LOH and CNV from DNA of human PDAC and PDAC cell lines have identified a number of potential loci of interest for pancreatic cancer (table 2). A systematic mutational screen of cancer genes is beeing carried out by several groups and coordinated by two major consortiums (ICGC and TCGA), and is leading to the identification of new cancer genes that might be relevant to pancreatic cancer. Recently UTX, a H3K27 demethylase has been found homozygously deleted in MIA-PaCa-2 cell line other than a variety of other solid tumors.

The resequencing of the kinase domain of all human Tyrosin Kynese genes in 11 pancreatic cancer cell lines and 29 microdissected primary tumors identified 6 nonsynonymous mutations in NTRK3, FGF3, PDGFRB, PTK6 and in the Src kinases YES1 and LYN (Kubo et al., 2009). Gene centered approaches such as exomic sequencing have provided not only candidate gene, but also a global view of how networks of driver mutations combine in to core signaling pathways by the extensive use of bioinformatic tools. The exome sequencing of sporadic PDAC identified about 2000 somatic mutations and more than 1600 copy number variations. Jones and colleague in 2008 refined those findings from exome sequencing of 29 cancers through bioinformatics tools. When combined with deletion/amplification data, adjusted for passenger mutation probabilities and analysed for pathways authors were able to identify 31 gene sets that could be grouped in 12 core signaling pathways altered in 67-100% of the analysed cancers. Furthermore the fact that the 31 gene sets were more enriched for differentially expressed genes, as analysed by SAGE, support the contribution of those signaling pathways. An interesting finding is that some pathway are characterized by predominating single or few gene mutations (e.g. KRAS, G1/S cell cycle transition and TGF-beta), might be more effectively targeted while others such as, integrin signaling, regulation of invasion, hemophilic cell adhesion, and GTPase dependent signaling have

different many genes are altered. Results from such a global approaches invite to reconsider how we combine target therapies, but also how we design targeted drug which should therefore target a physiologic effect rather than a single gene (Jones et al., 2008). Yachida and collegues further dissected data from seven patients of this cohort by mapping the distribution of mutations in different sections of the primary as well as of metastases. They were able to differentiate between founder mutations (i.e. mutations present in the founder clones and all the sequenced samples) and progressor mutations (i.e. not present in all the samples) accounting for about 64% and 36% respectively. Remarkably all mutations were represented in at least one part the primary tumor suggesting that heterogeneity of metastases reflect primary tumor heterogeneity. They also propose that metastases are a late event in pancreatic tumorigenesis, occurring only 2,7 years before death as compared to almost 18 years needed for the parental clone to arise. Despite its limited epidemiological significance this finding unveils a less aggressive nature of PDAC and should foster efforts to local control therapies paired to early biomarkers discovery. Data have been accumulating in the recent year and they highlight a limited number of frequently mutated genes (KRAS, TP53, CDKN2A, SMAD4, MLL3, TGFBR2, ARID1A and SF3B1). However some novel genes with a role in chromatin modification (EPC1 and ARID2), DNA damage repair

(ATM) and other mechanisms (ZIM2, MAP2K4, NALCN, SLC16A4 and MAGEA6) hold promises to unveil alternative pathways, as functional characterization in animal and cell models will be completed. An example is axon guidance and particularly the SLIT/ROBO signaling that emerged as frequently mutated in PDAC (Biankin et al, 2012).

Expression Profiling and taxonomy

A formal molecular taxonomy of pancreatic cancer has not been available until recently. Although not conclusive, three subtypes have been identified by combined analysis of transcriptional profiles of primary PDAC samples from different studies along with human and mouse PDA cell lines (Collison et al, 2011). Based on the specific gene expression profiles three subtypes were identified and designated as classical, quasimesenchimal (QM) and exocrine-like (EL). This classification did not show any correlation with histo-pathological characteristics (size, nodal involvement or grade) but classical subtypes showed significant better prognosis as compared to the two others. When investigated in human and mouse cell lines the EL subtype failed to be replicated, but clustering for classical and QU allowed identification of differential drug response to Gemcitabine and Erlotinib.

RNAseq has unveiled an unexpected genomewide deregulation of satellite expression that correlates with neuroendocrine features and enrichment of neuronal and stem cell satellite associated genes (Ting et al, 2010). Therefore, a definitive molecular taxonomy of PDAC will have to account for the emerging genetic and genomic and possibly epigenetic heterogeneity of PDAC (Jones 2008, Campbell 2010). On the other hand, efforts in the direction of defining subtypes of PDAC might encounter better luck into clinical practice due to the absence of widespread and easily detectable markers with prognostic and predictive value as in the case of breast cancer a well established gene expression signature struggle to overcome the determination of ER, PR and HER-2neu. It is foreseeable that patient stratification based on molecular subtypes will prove increasingly important as targeted therapies enter the arena of PDAC treatment.

Driver Pathways of PDAC

Kras

As stated above, KRAS mutations are a hallmark of PDAC. Kras is membrane-bound GTP binding protein that, when activated by signaling partners, (e.g.: epidermal growth factor receptor, EGFR),

releases GDP in exchange for GTP ("on" state), and activates downstream signaling events, such as the Raf, MAP2K, MAPK and the PI3K–Akt cascades. Mutations in KRAS, impair the intrinsic GTPase activity required to switch "off" the active GTP-bound state. The nature of this mutation made KRAS an elusive target, and therapeutic strategies have focused on Kras post-translational modification enzymes (franesyl and geranyltransferases) or a number of upstream and downstream targets. Alternative approaches to Kras therapies include peptide vaccine to stimulate immunity against mutant RAS, or RNA-directed gene silencing with RNAi or antisenses nucleotide. Many of those agents are now in clinical trials and their efficacy needs further investigations (reviewed in Wong et al, 2009). The evidence that in other carcinomas such as colorectal and lung adenocarcinomas, KRAS mutations occur at a lower rate (50% and 25%, respectively) rises the question whether a definite pattern of oncogene cooperativity and context dependent Kras driven tumorigenesis exist (Tuveson, 2004, Guerra 2003, Barbacid, 2003 – not the best reference). This point has been addressed by different approaches and models (Tuveson, 2004, Guerra 2003, Hingorani 2003). A common observation was that, in the presence of an intact p19ARF/p53 pathway, overexpression of Kras induces senescence i*n vitro*. Subsequently, it has become clear that endogenous levels of oncogenic Kras are autonomously able to initiate transformation by

stimulating proliferation in the earliest stages of PDAC in mouse (Tuveson, 2004). Consistently, Kras amplification only occurs later in tumor progression (Bos, 1988). However, the clustered pattern of mutations seen in PDAC and the evidence of a p53 dependent survival of KrasG12D/+ pancreatic ductal cells still support a pre-ordered path of escape oncogenic Kras induced senescence trough inactivation of either p53 or p16 (Serrano, 1997; Guerra 2003; Morton, 2010).

The effort to recapitulate p53 inactivation offers a similar example of the profound biological differences offered by models with a different degree of proximity to the physiological conditions. In the context of $Kras^{G12D}$ the activity of a dominant negative mutated p53 allele (LSL-$Trp53^{R172H}$) is able to recapitulate in mouse the aggressive metastatic behavior that characterize PDAC in human (Hingorani, 2005, Morton, 2010), a feature not commonly observed in mice with the loss p53 allele. Indeed the expression of $Trp53^{R172H}$ dominant negative allele is likely to reproduce more accurately the genetic event that leads to a stabilized form of the protein (commonly detected as p53 overexpression at IHC), suggesting a gain of function mechanism. Despite the exact mechanism of this gain of function remains unclear, it has been shown that “oncogenic” p53 determine complex structural chromosomal instability in a telomere

independent manner (Hingorani, 2005) and corroborate the idea of a cooperative role of mutated Kras in expanding a pool of progenitor cells that in the context of this allele develop LOH of the wild type p53 (Hingorani, 2005; Hingoran.i 2003). Intriguingly this suggests that oncogenic p53 might contribute to establish the chromosomal instability required to develop LOH, a common mechanism for tumor suppressor loss, p53 included, in PDAC (Rozenblum, 1997; Scarpa, 1993, Tuveson 2005). A different mechanism of progression involves p53 suppression of p21 that mediates the growth arrest/senescence response as shown by the lack of invasive PDAC development in a p53 mutant allele able to transactivate p21 (Morton, 2010; el-Deiry 1994; Liu, 2004; Ludwig 1996).

Despite the role of Kras in PDAC initiation and maintenance is well established, the effort to identify whether Kras might become dispensable along progression has led to the identification of signatures of Kras dependency or addiction in PDAC and other Kras driven tumors (Sing, 2009). Upon Kras knowkdown, Kras-mutant cancer cell lines show diverse levels of Kras addiction, which seems to correlate with the expression of proteins such as Syk and Ron kinases and integrin beta 6. Interestingly loss of Kras addiction is linked to the induction of epithelial-mesenchymal transformation (EMT), a cellular phenotype observed also upon TGF-beta activation impaired in about

50% of PDAC by homozigous deletion of the TGFbeta pathway component SMAD4. This may suggest a cooperative role of TGFbeta signaling loss in maintaining Kras dependency in well-differentiated PDAC (Hezel et al, 2006; Bardeesy et al, 2006, Sing et al, 2009). Wider approaches with high-throughput RNA interference (RNAi) to identify synthetic lethal interactions in Kras mutant cancer cells, have identified STK33, a serine/threonine kinase responsible for mitochondrial apoptosis suppression, as an alternative Kras co-dependent pathway in cancer cell lines driven by mutant Kras (School et al, 2009). Similarly PITX1 was identified as a suppressor of Ras activity and tumorigenicity possibly acting through RASAL1 from a RNAi library screening (Kolfschoten, 2006). Despite the specific relevance of these circuitries for PDAC must be further exploited, RNAi based approaches have the potential to unveil novel pathways.

Relevance of Kras signaling to MEK and PI3-Kinase is described in Chapter 3.

Smad4/TGFbeta

Transforming growth factor (TGF)-beta is part of a superfamily of growth factors that signals through serine/threonine kinase receptor complexes and in turns phosphorylate receptor-regulated Smad proteins (SMAD2, SMAD3, and the obligate binding partner SMAD4)

Their role is to regulate a variety of cellular functions including proliferation, differentiation, migration, and apoptosis. A clear-cut understanding the role of TGF-beta in PDAC has remained elusive because of a plethora of reports indicating growth-inhibitory and growth-promoting effects depending on the cell type and cell context and the existence of a SMAD independent signaling. The well established and common genetic loss of SMAD4 and antiangiogenetic and stromal effect of its restoration in xenograft account only in part for the role of TGFbeta in PDAC (Schwarte-Waldhoff et al. 2000; Peng et al. 2002; Duda et al. 2003).

Among SMAD independent functions of TGFbeta, EMT has emerged as a well described feature in mouse models and human PDAC (Bardeesy et al, 2006; Hingorani et al, 2005, Levy and Hill, 2005). EMT is characterized by actin reorganization, loss of adherent junctions and the acquisition of a mesenchymal phenotype that resemble the high grade histologic features more commonly found in advanced PDAC (Iacobuzio-Donahue et al 2010; Kamisawa et al 2004). This feature is not predicted by any histopathological feature of the early cancer, neither correlates with Smad4 loss suggesting the requirement of other effectors (Iaccobuzio-Donahue 2010; Kamisawa 2004). Indeed, PI3K and PTEN have been shown to act synergistically with TGFbeta down-regulating E-cadherin and basal cell adhesion

(Vogelmann et al, 2005). Interestingly PTEN seems to be linked to TGFbeta also in a SMAD4 dependent manner. Upon conditional homozygous loss of the Smad4 allele no PDAC is developed, while an increase in PTEN is seen. In the background of PTEN mutation Smad4 null mice show activation of Notch1 related transdifferentiation of acinar, centroacinar and islet cells, and development of high pATK and mTOR PDAC, a feature present in the majority of the human counterparts (Dawnward, 2005; Xu 2010).

Hedgehog-Smo-Gli

The ligand-dependent Hedgehog (Hh) signaling is a well characterized embryonic developmental pathway that has been consistently implicated in a number of solid tumors including PDAC. The role of this pathway rely on the paracrine action of three mammalian Hh homologs, namely DHH, IHH and SHH. Hh signaling involves the release of the oncogenic transmembrane protein SMO by the tumor suppressor PTC1 upon binding of Hh protein and the SMO dependent expression of specific Hh genes such as GLI1. The use of Shh mouse model (Pdx-Shh) and Hh pharmacological inhibitors such as cyclopamine have shed light on complex role of this pathway in PDAC involving both non cell-autonomous and cell-autonomous

tumorigenic mechanism (PI3K-Akt, stabilization of Bcl2 and BclXL). In human, SHH is expressed in 70% of PDAC and in PanIN 1-3 and absent in normal pancreata. In addition other Hh signaling components such as IHH, Smo, and PTC1 show various degree of deregulation (Thayer, 2003; Berman, 2003, Kayed 2004). Moreover cyclopamine is able to induce growth arrest in PDAC cell line, suggesting an early and cell autonomous role of Hh signaling (Thayer et al, 2003). Interestingly, Pdx-Shh mouse display PanIN-like abnormalities through both epithelial changes and acinar metaplasia together with early accumulation of Ras mutations and overexpression of HER-2/*neu* (Thayer et al, 2003). In contrast, the recent demonstration of enhancement of drug intratumoral concentration and response to Doxorubicine and Gemcitabine upon SMO inihibition in the a dominant negative p53 PDAC mouse model (KPC) prompted a shift of interest to stroma as a Hh targetable physical and biological player of PDAC chemoresistance (Tuveson et al., 2009). Indeed, SMO inhibition lead to depletion of desmoplastic stroma, and increase of vessel density, a mechanism mediated, at least partially, by the Gli family of transcription factors (Tuvesonet al, 2009, Yauch et al, 2008). Moreover, inhibition of Hh signaling in the mouse stroma results in growth inhibition in xenograft tumour models and activation of tumor promoting Hh targets genes is restricted to tumor stroma supporting a paracrine requirement for

Hh ligand signalling in the tumorigenesis of Hh-expressing PDACs (Tian et al, 2009; Yauch et al, 2008). It is likely that stroma doesn't totally account for chemo resistance in PDAC as confirmed by the observation that the expression of Gli target genes is maintained in Smo-negative ducts and that Gli transcription is decoupled from upstream Shh–Ptch–Smo signaling and is regulated by TGF-b and KRAS (Nolan Stevaux, 2008). In fact, available therapies fail in metastatic localizations that are characterized by a lesser amount of stroma (Hidalgo, 2009). It should be noted how in such a rapidly progressing and often unresectable disease, the biology of advanced stage PDAC in human is still poorly understood. Nonetheless, Hh pathway offers a privileged point of view that might help to explain several emerging mechanism of cancer cell biology (e.g. epithelia-to mesenchima transition, EMT), and the complex crosstalk with microenvironment (Wnt, IGF like receptors, Yauch 2008). Importantly, we are awaiting results from early phase clinical trials to understand the potential use of Hh inhibitors in stroma rich tumors such as PDAC (Wong 2009).

Scope of the thesis

As new-targeted agents are becoming available for clinical trial we aimed to design improved therapeutic approaches for the treatment of pancreatic ductal adenocarcinoma by means of in vitro and in vivo models of pancreatic adenocarcinoma.

We analysed the results of a high-throughput screening of >500 human cancer cell lines (including 46 PDAC lines), for sensitivity to 50 clinically relevant compounds.

We designed two different strategies including a JAK2 inhibitor that blocks STAT3 function (Chapter 2) and a MEK1/2 inhibitor, AZD-6244, for efficacy alone or in combination with the PI3K inhibitors, BKM-120 or GDC-0941 (Chapter 3), in a $KRAS^{G12D}$-driven GEMM that recapitulates the multi-step progression of human PDAC.

Bibliography

1. Aguirre AJ, Brennan C, Bailey G, Sinha R, Feng B, Leo C, Zhang Y, Zhang J, Gans JD, Bardeesy N, Cauwels C, Cordon-Cardo C, Redston MS, DePinho RA, Chin L. High-resolution characterization of the pancreatic adenocarcinoma genome. Proc Natl Acad Sci U S A. 2004 Jun 15;101(24):9067-72.
2. Al-Sukhni, W.; Rothenmund, H.; Eppel Borgida, A.; Zogopoulos, G.; O'Shea, A.-M.; Pollett, A.; Gallinger, S. Germline BRCA1 mutations predispose to pancreatic adenocarcinoma. Hum. Genet. 124: 271-278, 2008.
3. Biankin AV, Waddell N, Kassahn KS, Gingras MC, Muthuswamy LB, Johns AL, Miller DK, Wilson PJ, Patch AM, Wu J, Chang DK, Cowley MJ, Gardiner BB, Song S, Harliwong I, Idrisoglu S, Nourse C, Nourbakhsh E, Manning S, Wani S, Gongora M, Pajic M, Scarlett CJ, Gill AJ, Pinho AV, Rooman I, Anderson M, Holmes O, Leonard C, Taylor D, Wood S, Xu Q, Nones K, Fink JL, Christ A, Bruxner T, Cloonan N, Kolle G, Newell F, Pinese M, Mead RS, Humphris JL, Kaplan W, Jones MD, Colvin EK, Nagrial AM, Humphrey ES, Chou A, Chin VT, Chantrill LA, Mawson A, Samra JS, Kench JG, Lovell JA, Daly RJ, Merrett ND, Toon C, Epari K, Nguyen NQ, Barbour A, Zeps N; Australian Pancreatic Cancer Genome Initiative, Kakkar N, Zhao F, Wu YQ, Wang M, Muzny DM, Fisher WE, Brunicardi FC, Hodges SE, Reid JG, Drummond J, Chang K, Han Y, Lewis LR, Dinh H, Buhay CJ, Beck T, Timms L, Sam M, Begley K, Brown A,

Pai D, Panchal A, Buchner N, De Borja R, Denroche RE, Yung CK, Serra S, Onetto N, Mukhopadhyay D, Tsao MS, Shaw PA, Petersen GM, Gallinger S, Hruban RH, Maitra A, Iacobuzio-Donahue CA, Schulick RD, Wolfgang CL, Morgan RA, Lawlor RT, Capelli P, Corbo V, Scardoni M, Tortora G, Tempero MA, Mann KM, Jenkins NA, Perez-Mancera PA, Adams DJ, Largaespada DA, Wessels LF, Rust AG, Stein LD, Tuveson DA, Copeland NG, Musgrove EA, Scarpa A, Eshleman JR, Hudson TJ, Sutherland RL, Wheeler DA, Pearson JV, McPherson JD, Gibbs RA, Grimmond SM. Pancreatic cancer genomes reveal aberrations in axon guidance pathway genes. Nature. 2012 Nov 15;491(7424):399-405.

4. C. Almoguera, D. Shibata, K. Forrester, J. Martin, N. Arnheim and M. Perucho, Most human carcinomas of the exocrine pancreas contain mutant c-K-ras genes, *Cell* **53** (1988), pp. 549–554.
5. Calhoun, E.S., Jones, J.B., Ashfaq, R., Adsay, V., Baker, S.J., Valentine, V., Hempen, P.M., Hilgers, W., Yeo, C.J., Hruban, R.H., et al. BRAF and FBXW7 (CDC4, FBW7, AGO, SEL10) mutations in distinct subsets of pancreatic cancer: Potential therapeutic targets. *Am. J. Pathol.* 2003. **163:** 1255–1260.
6. Chin L, Artandi SE, Shen Q, Tam A, Lee SL, Gottlieb GJ, Greider CW, DePinho RA. p53 deficiency rescues the adverse effects of telomere loss and cooperates with telomere dysfunction to accelerate carcinogenesis. Cell. 1999 May 14;97(4):527-38.

7. Cubilla AL, Fitzgerald PJ. Morphological lesions associated with human primary invasive nonendocrine pancreas cancer. Cancer Res 1976;36:2690 – 8.
8. Feldmann G, Beaty R, Hruban RH, Maitra A. Molecular genetics of pancreatic intraepithelial neoplasia. J Hepatobiliary Pancreat Surg. 2007;14(3):224-32. Epub 2007 May 29.
9. Gisselsson, D., Jonson, T., Petersen, A., Strombeck, B., Dal Cin, P., Hoglund, M., Mitelman, F., Mertens, F., and Mandahl, N. Telomere dysfunction triggers extensive DNA fragmentation and evolution of complex chromosome abnormalities in human malignant tumors. *Proc. Natl. Acad. Sci.* 2001. **98:** 12683–12688.
10. Hashimoto Y, Murakami Y, Uemura K, Hayashidani Y, Sudo T, Ohge H, Fukuda E, Shimamoto F, Sueda T, Hiyama E. Telomere shortening and telomerase expression during multistage carcinogenesis of intraductal papillary mucinous neoplasms of the pancreas. J Gastrointest Surg. 2008 Jan;12(1):17-28
11. Heinmoller, E. et al. Molecular analysis of microdissected tumors and preneoplastic intraductal lesions in pancreatic carcinoma. Am. J. Pathol. 157, 83–92 (2000).
12. Hingorani SR, Wang L, Multani AS, Combs C, Deramaudt TB, Hruban RH, Rustgi AK, Chang S, Tuveson DA. Trp53R172H and KrasG12D cooperate to promote chromosomal instability and widely metastatic pancreatic ductal adenocarcinoma in mice. Cancer Cell. 2005 May;7(5):469-83.

13. Hruban RH, Adsay NV, Albores-Saavedra J, et al. Pancreatic intraepithelial neoplasia: a new nomenclature and classification system for pancreatic duct lesions. Am J Surg Pathol 2001;25:579– 86.
14. Ishimura, N., Yamasawa, K., Karim Rumi, M.A., Kadowaki, Y., Ishihara, S., Amano, Y., Nio, Y., Higami, T., and Kinoshita, Y. BRAF and K-ras gene mutations in human pancreatic cancers. *Cancer Lett. 2003.* **199:** 169–173.
15. Karhu R, Mahlamäki E, Kallioniemi A. Pancreatic adenocarcinoma -- genetic portrait from chromosomes to microarrays. Genes Chromosomes Cancer. 2006 Aug;45(8):721-30.
16. Klimstra DS, Longnecker DS. K-ras mutations in pancreatic ductal proliferative lesions. Am J Pathol. 1994 Dec;145(6):1547-50.
17. Levy L, Hill CS. Smad4 dependency defines two classes of transforming growth factor {beta} (TGF-{beta}) target genes and distinguishes TGF-{beta}-induced epithelial-mesenchymal transition from its antiproliferative and migratory responses. Mol Cell Biol. 2005 Sep;25(18):8108-25.
18. Lohr M, Kloppel G, Maisonneuve P, Lowenfels AB, Luttges J. Frequency of K-ras mutations in pancreatic intraductal neoplasias associated with pancreatic ductal adenocarcinoma and chronic pancreatitis: a meta-analysis. Neoplasia 2005;7:17–23.

19. Lowenfels, A. B., Maisonneuve, P., Whitcomb, D. C., Lerch, M. M. & DiMagno, E. P. Cigarette smoking as a risk factor for pancreatic cancer in patients with hereditary pancreatitis. *JAMA* 286, 169–170 (2001).
20. Luttges J, Diederichs A, Menke MA, Vogel I, Kremer B, Kloppel G. Ductal lesions in patients with chronic pancreatitis show K-ras mutations in a frequency similar to that in the normal pancreas and lack unclear immunoreactivity for p53. Cancer 2000; 88:2495–504.
21. Maser, R.S. and DePinho, R.A. Connecting chromosomes, crisis, and cancer. *Science.* 2002 **297:** 565–569.
22. McWilliams, R. R.; Rabe, K. G.; Olswold, C.; De Andrade, M.; Petersen, G. M. Risk of malignancy in first-degree relatives of patients with pancreatic carcinoma. Cancer 104: 388-394, 2005.
23. Medicherla S, Li L, Ma JY, Kapoun AM, Gaspar NJ, Liu YW, Mangadu R, O'Young G, Protter AA, Schreiner GF, Wong DH, Higgins LS. Antitumor activity of TGF-beta inhibitor is dependent on the microenvironment. Anticancer Res. 2007 Nov-Dec;27(6B):4149-
24. Pogue-Geile, K. L.; Chen, R.; Bronner, M. P.; Crnogorac-Jurcevic, T.; Moyes, K. W.; Dowen, S.; Otey, C. A.; Crispin, D. A.; George, R. D.; Whitcomb, D. C.; Brentnall, T. A. Palladin mutation causes familial pancreatic cancer and suggests a new cancer mechanism. PLoS Med. 3: e516, 2006.
25. Rasheed ZA, Yang J, Wang Q, Kowalski J, Freed I, Murter C,

Hong SM, Koorstra JB, Rajeshkumar NV, He X, Goggins M, Iacobuzio-Donahue C, Berman DM, Laheru D, Jimeno A, Hidalgo M, Maitra A, Matsui W. Prognostic significance of tumorigenic cells with mesenchymal features in pancreatic adenocarcinoma. J Natl Cancer Inst. 2010 Mar 3;102(5):340-51.

26. Robertson, K. D.; Jones, P. A. Tissue-specific alternative splicing in the human INK4a/ARF cell cycle regulatory locus. *Oncogene* 18: 3810-3820, 1999.
27. Rovira M, Scott SG, Liss AS, Jensen J, Thayer SP, Leach SD. Isolation and characterization of centroacinar/terminal ductal progenitor cells in adult mouse pancreas. Proc Natl Acad Sci U S A. 2010 Jan 5;107(1):75-80.
28. Rozenblum E, Schutte M, Goggins M, Hahn SA, Panzer S, Zahurak M, Goodman SN, Sohn TA, Hruban RH, Yeo CJ, Kern SE. Tumor-suppressive pathways in pancreatic carcinoma. Cancer Res. 1997 May 1;57(9):1731-4
29. Shi C, Hong SM, Lim P, Kamiyama H, Khan M, Anders RA, Goggins M, Hruban RH, Eshleman JR. KRAS2 mutations in human pancreatic acinar-ductal metaplastic lesions are limited to those with PanIN: implications for the human pancreatic cancer cell of origin. Mol Cancer Res. 2009 Feb;7(2):230-6. Epub 2009 Feb 10.
30. Shi C, Hong SM, Lim P, Kamiyama H, Khan M, Anders RA, Goggins M, Hruban RH, Eshleman JR. KRAS2 mutations in human pancreatic acinar-ductal metaplastic lesions are

limited to those with PanIN: implications for the human pancreatic cancer cell of origin. Mol Cancer Res. 2009 Feb;7(2):230-6. doi: 10.1158/1541-7786.MCR-08-0206.

31. Slater, E. P. *et al*. PALB2 mutations in European familial pancreatic cancer families.*Clin. Genet.* 78, 490–494 (2010). *Nature Reviews Cancer* 13, 66-74 (January 2013) | doi:10.1038/nrc3420

32. Tischkowitz, M. D. *et al*. Analysis of the gene coding for the BRCA2-interacting protein PALB2 in familial and sporadic pancreatic cancer. *Gastroenterology* 137, 1183–1186 (2009).
33. Wilentz, R. E. et al. Loss of expression of Dpc4 in pancreatic intraepithelial neoplasia: evidence that DPC4 inactivation occurs late in neoplastic progression. Cancer Res. 60, 2002–2006 (2000).
34. Wong and Lemoine. Pancreatic cancer: molecular pathogenesis and new therapeutic targets. Nat Rev Gastroenterol Hepatol (2009) vol. 6 (7) pp. 412-22
35. Xu X, Ehdaie B, Ohara N, Yoshino T, Deng CX.Synergistic action of Smad4 and Pten in suppressing pancreatic ductal adenocarcinoma formation in mice. Oncogene. 2010 Feb 4;29(5):674-86.

***STAT3* plays a critical role in *KRAS*-induced pancreatic tumorigenesis**

Ryan B. Corcoran,1,2 Gianmarco Contino,1,2 Vikram Deshpande,3 Alexandros Tzatsos,1,2 Claudius Conrad,1 Cyril H. Benes,1,2 Jeffrey Settleman,1,2 Jeffrey A. Engelman,1,2 and Nabeel Bardeesy1,2

1Massachusetts General Hospital Cancer Center, Boston, MA 02129, USA

2Department of Medicine, Harvard Medical School, Boston, MA 02115, USA

3Department of Pathology, Massachusetts General Hospital and Harvard Medical School, Boston, MA 02115, USA

Abstract

The STAT3 transcription factor is an important regulator of stem cell self-renewal, cancer cell survival, and inflammation. In the pancreas, STAT3 is dispensable for normal development whereas the majority of pancreatic ductal adenocarcinomas (PDAC) show constitutive activation of STAT3, suggesting its potential as a therapeutic target in this cancer. Here, we sought to define the mechanisms of STAT3 activation and its functional importance in PDAC pathogenesis. Large-

scale screening of cancer cell lines with a JAK2 inhibitor that blocks STAT3 function revealed a >30-fold range in sensitivity in PDAC, and showed a close correlation of sensitivity with levels of tyrosine-phosphorylated STAT3 and of the gp130 receptor, an upstream signaling component. Correspondingly, upregulation of the IL6/LIF-gp130 pathway accounted for the strong STAT3 activation in PDAC subsets. To define functions of STAT3 in vivo, we developed mouse models that test the impact of conditional inactivation of STAT3 in KRAS-driven PDAC. We showed that STAT3 is required for the development of the earliest pre-malignant pancreatic lesions, acinar-to-ductal metaplasia (ADM) and pancreatic intraepithelial neoplasia (PanIN). Moreover, acute STAT3 inactivation blocked PDAC initiation in a second in vivo model. Our results demonstrate that STAT3 has critical roles throughout the course of PDAC pathogenesis, supporting the development of therapeutic approaches targeting this pathway. Moreover, our work suggests that gp130 and phospho-STAT3 expression may be effective biomarkers for predicting response to JAK2 inhibitors.

Keywords: Pancreatic cancer, STAT3, Pancreatic intraepithelial neoplasia, mouse models, gp130

INTRODUCTION

Pancreatic ductal adenocarcinoma (PDAC) is the fourth leading cause of cancer death in the United States and carries a dismal 5-year survival rate of <5% (1). Activating mutations in the KRAS oncogene are the defining lesion in this malignancy, present in 70–95% of cases (2–4). PDAC is believed to arise from precursor lesions called pancreatic intraepithelial neoplasia (PanIN). Molecular pathology analysis of human specimens and the development of genetically engineered mouse models support a model in which PanINs proceed through multiple stages of increasingly severe cellular atypia culminating in the development of invasive carcinoma. This histologic progression is associated with KRAS activation as an early event and the subsequent step-wise accumulation of inactivating mutations in the tumor suppressors, Ink4a/Arf, p53, and SMAD4 (5,6). As this genetic information has not yet led to the development of effective targeted therapeutic strategies in PDAC, there is considerable focus on defining additional molecular pathways driving the progression and maintenance of this disease.f

The Signal transducer and activator of transcription (STAT) family transcription factors are constitutively activated in a wide range of

human malignancies (7). STAT proteins are present in the cytoplasm under basal conditions and are activated by phosphorylation on a single tyrosine residue, which triggers dimerization and nuclear localization (8,9). Classically, STAT tyrosine phosphorylation is mediated by the Janus (JAK) family of tyrosine kinases, which themselves are activated by cytokine and growth factor receptors (10,11). Other tyrosine kinases, such as src, have also been reported to mediate tyrosine phosphorylation of STAT proteins (12). The STAT proteins were originally identified as factors required for downstream signaling in response to interferon and other inflammatory cytokines (8). Subsequent studies identified key functions for STAT proteins in the maintenance of self-renewal of embryonic stem cells and in the activation of proliferative, anti-apoptotic and inflammatory pathways to initiate and maintain growth of a number of tumor types (7,13,14).

STAT3 has been identified as a key oncogenic factor in a number of epithelial malignancies and is required for oncogenesis in mouse models of skin and gastric cancers (15,16). In PDAC, constitutive activation of STAT3 by phosphorylation of Tyr705 has been reported in 30–100% of human tumor specimens, as well as in many PDAC cell lines (17,18). By contrast, this pathway is inactive in normal pancreas,

and correspondingly STAT3 is not required for pancreatic development or homeostasis, as demonstrated by conditional knockout studies in mice (19). Several lines of evidence suggest that aberrant activation of STAT3 in PDAC is functionally important. Firstly, STAT3 is required for the process of acinar-to-ductal metaplasia (ADM)—thought to be an early event in PDAC pathogenesis—upon ectopic expression of the Pdx1 transcription factor, a key regulator of early pancreatic development (20). In addition to this potential role in early PDAC, STAT3 has been suggested as a therapeutic target in established PDAC since examination of a limited number of cell lines for the impact of chemical STAT3 pathway inhibitors and dominant-negative STAT3 constructs has shown that the pathway may contribute to the proliferation of some PDAC cell lines in vitro and the tumorigenicity of some PDAC xenografts (17,18,21,22). These data support the need for more detailed studies to define the basis for STAT3 activation in PDAC and to rigorously establish specific roles for STAT3 in the initiation and progression of PDAC in vivo.

In this study, we examined the sensitivity of a large series of PDAC cells lines to pharmacologic STAT3 inhibition and defined biomarkers of sensitivity as well as key upstream activators of the pathway in this

cancer. We also employed genetically engineered mouse models to determine the impact of genetic inactivation of STAT3 on the progression of PDAC. Collectively our results demonstrate that upregulation of the gp130 receptor and strong STAT3 phosphorylation point to a subset of PDAC that are highly sensitive to pharmacologic inhibition of the JAK2/STAT3 pathway, and that STAT3 plays an important role in driving PDAC progression at multiple stages of pancreatic tumorigenesis in vivo, thereby supporting STAT3 as a potential therapeutic target in PDAC.

MATERIALS AND METHODS

Cell Lines

PDAC cell lines were grown in DMEM/F12 (GIBCO) with 10% FBS and assayed in DMEM/F12 with 5% FBS and were obtained from the MGH Center for Molecular Therapeutics (CMT), which performs routine cell line authentication testing by SNP and STR analysis. For drug sensitivity studies, data from over 500 solid tumor cell lines were obtained from the CMT drug screen database (30). Viable cell titer relative to untreated cells was determined using Cell Titer Glo assay (Promega). For apoptosis assays, cells were stained with propidium

iodide and Annexin V Cy5 (Biovision) according to the manufacturer's protocol and assayed on a LSRII flow cytometer (BD Biosciences).

Mouse Strains and Histologic Analysis

The Pdx1-Cre transgenic mouse strain and the LSL-KRASG12D knock-in mouse strain have been previously described (23,24). The STAT3lox/lox mouse strain was kindly provided by David Levy (25). These strains were intercrossed to produce the experimental cohorts. Pancreata isolated from 12 week-old mice were analyzed in blinded fashion by a single pathologist (V.D.) to determine the percent of each pancreas occupied by ADM or PanIN lesions.

Pancreatic ductal cells

Pancreatic ductal cells where isolated from 9 week-old Pdx1-Cre; LSL-KRASG12D mice as previously described (26) and propagated in laminin (BD Biosciences). Mouse shp53 retroviral construct (MLS sh-p53.1224, 27) was transfected in Ecopack 293T cells and media collected at 48 and 72 hours. One week after overnight incubation

with retrovirus in the presence of 8μg/mL polybrene, GFP-positive infected cells were FACS-sorted and propagated.

Molecular Analyses

Western blotting was performed using standard methods. Immunostaining was performed using standard methods on formalin-fixed, paraffin embedded tissues. After deparaffinization slides are washed with 9.83% NaCl for 3 min followed by a PBS wash and a wash in distilled water for 5min. Antigen retrieval was performed with pressure cooker (2100 Retriever, PickCell Laboratories) and R-Buffer A (pH6.0, Electron Microscopy Sciences).

Orthotopic tumor model

SCID mice (C3SnSmn.CB17-Prkdcscid/J, Jackson Labs) were subjected to general anesthesia according to MGH SRAC policies. Orthotopic injections of the pancreas were performed as previously described (28), using 2×104 PanIN cells suspended in 50μl of Duct Media (26), mixed with 50μl of Matrigel (BD Biosciences).

Results

Phospho-STAT3 levels predict the sensitivity of PDAC cell lines to JAK2 inhibition

Previous studies of a limited number of human PDAC cell lines have shown that subsets are sensitive to pharmacologic or genetic inactivation of the JAK2/STAT3 pathway (17,18,21). To more broadly define the role of this pathway in PDAC tumor maintenance, we evaluated the drug sensitivity profile for the JAK2-selective inhibitor AZ960 across a large-scale cell line repository containing over 500 solid tumor cell lines, including 46 PDAC cell lines (29,30). These cell lines are characterized at the molecular level for regional changes in chromosomal copy number (SNP Chip analysis), global mRNA expression, and common cancer gene mutations, enabling correlations of sensitivity in relation to specific molecular features. PDAC cell lines as a group showed intermediate sensitivity to JAK2 inhibition (Fig. 1A). However, we found that a subset (20%) of PDAC cell lines displayed high sensitivity (>75% inhibition of viable cell number relative to untreated control), suggesting that JAK2 inhibitors could be useful in selected PDAC patients. To explore this possibility further, we evaluated P-STAT3 levels in a panel of 10 randomly selected PDAC cell lines (Fig. 1B). While P-STAT3 could be detected in all but one cell line, high levels of P-STAT3 in comparison with normal

pancreatic tissue were detected in 4 of the 10 cell lines; these high levels in cell lines were comparable to those observed in PDAC tissue specimens.

Notably, there was a strong correlation between high levels of P-STAT3 and sensitivity to AZ960 (Fig. 1B, and Supplementary Fig. S1). In cell lines with elevated P-STAT3, AZ960 inhibited cell viability in a dose-dependent manner that correlated with inhibition of STAT3 Tyr705-phosphorylation (Fig. 1C). This was associated with down-regulation of BclXL (Fig. 1D), an anti-apoptotic protein and an established STAT3 target (29), as well as a corresponding pronounced induction of apoptosis. By contrast, cell lines with low P-STAT3 showed no changes in P-STAT3 or BclXL in response to AZ960, and did not undergo apoptosis, suggesting that low basal levels of STAT3 Tyr705-phosphorylation in these cell lines are not due to JAK2 (Figs. 1C, D). As expected, AZ960 did not affect STAT3 Ser727-phosphorylation (Fig. 1D), a modification known to be JAK2-independent (31,32). These data indicate that strong STAT3 activation seen in a subset PDAC cell lines is mediated by JAK2 and may predict sensitivity to JAK2 inhibitors.

IL-6 family cytokine signaling regulates P-STAT3 levels in PDAC cell lines

Next, we sought to establish the upstream signaling pathways responsible for STAT3 activation in PDAC. To this end, we took advantage of the genome-wide mRNA expression profiles available for our cell line repository to identify transcripts enriched in PDAC cell lines with elevated P-STAT3 levels. This analysis identified 126 transcripts associated with strong STAT3 activation. We cross-referenced this gene set with a list of 30 genes identified by a gene ontology search as positive regulators of STAT3 tyrosine phosphorylation (Figs. 2A, Supplementary Fig. S2). Notably, the only gene found to be present in both gene sets was the interleukin 6 signal transducer (IL6ST), which encodes membrane glycoprotein 130 (gp130). This protein is the common signal transducing component of the IL6 cytokine receptor family, which forms complexes with the ligand-binding receptor subunits of multiple IL6 cytokine family members (including the IL6, leukemia inhibitory factor (LIF), oncostatin M, and ciliary neurotrophic factor receptors), thereby serving as an important activator of JAK-STAT signaling (33,34). Significantly, the level of IL6ST transcript in PDAC cell lines was strongly correlated with the degree of sensitivity to the JAK2 inhibitor AZ960 in our large-scale cell line screen (Fig. 2B). This effect was specific to JAK-STAT pathway inhibition, as IL6ST transcript levels showed no correlation with sensitivity to inhibitors of EGFR, MEK1/2, and IGF1R (using erlotinib, AZD6244, and AEW541, respectively;

Supplementary Fig. S3), pathways that are under active investigation as PDAC drug targets. While the mechanism of IL6ST upregulation in PDAC cell lines is not clear—no focal gene amplifications were detected, and Stat3 knockdown (Fig. S4), these data show that IL6ST transcript levels specifically predict sensitivity to JAK2 inhibition in PDAC cell lines, and suggest that IL6ST may be a key upstream mediator of JAK-STAT3 activity in this cancer.

To test directly whether IL6ST signaling regulates P-STAT3 in PDAC cell lines, cells were treated with a monoclonal neutralizing antibody to gp130, known to block signaling by multiple IL6 cytokine family members (35). This antibody inhibited P-STAT3 in a dose-dependent manner in PDAC cell lines with high P-STAT3 levels, while only modestly affecting basal levels in low P-STAT3 lines (Fig. 2C). Since these findings suggest that IL6 cytokine family signaling through IL6ST regulates STAT3 activation in PDAC cell lines, we evaluated the expression of IL6 cytokine family members in human PDAC, in comparison to normal pancreas. Consistent with our cell line data, IL6ST transcript levels were significantly increased in PDAC, relative to normal pancreas, whereas levels of IL6R and LIFR/CD118 were not up-regulated in PDAC tissue. Transcript levels of IL6 cytokine family ligands IL6 and LIF were also significantly increased in PDAC, relative

to normal pancreas. Thus, upregulation of gp130 and IL6/LIF are likely to contribute to STAT3 activation in human PDACs.

STAT3 phosphorylation is observed at multiple stages of KRAS-induced pancreatic tumorigenesis

Since some PDAC cell lines appear to be highly dependent on STAT3 activity, we chose to explore the contributions of STAT3 to different stages PDAC evolution in vivo. First, we sought to establish the tyrosine-phosphorylation status of STAT3 at different stages of PDAC pathogenesis. We employed a genetically engineered model of multi-stage tumor progression (Pdx1-Cre; LSL-KRASG12D mice) in which activation of an oncogenic KRASG12D allele in the pancreas results in gradual formation of ADM and PanIN lesions. PanINs progress to PDAC with long latency (~1 year), which is greatly accelerated by genetic inactivation of the p53 or Ink4a/Arf tumor suppressor loci (24,36–38). Immunofluorescence analysis showed that P-STAT3 staining was undetectable in normal pancreas. By contrast, nuclear P-STAT3 expression was present at all stages of PDAC progression, with robust staining observed in both ADM and PanINs (Figs. 3A, B) as well as in fully developed invasive PDAC, consistent with elevated P-STAT3 levels in tumor tissue seen by western blot analysis (Fig. 1B). At each

stage of tumorigenesis, there was also evidence of sporadic P-STAT3 staining in the stromal tissue. Thus, STAT3 activation occurs at the earliest stages of pancreatic tumorigenesis and is maintained in invasive cancers, implying possible roles for STAT3 in both tumor initiation and in continued propagation of advanced PDAC. Additionally, the staining pattern may indicate functions of STAT3 in both the tumor epithelium and stroma.

Loss of STAT3 reduces ADM and PanIN formation induced by oncogenic KRAS

ADM is the earliest change observed in models of KRAS-induced pancreatic oncogenesis and is a potential precursor to PanIN (39,40). Based on the expression pattern of P-STAT3 in these lesions, we examined the requirement of STAT3 in early pancreatic tumorigenesis by crossing Pdx1-Cre; LSL-KRASG12D mice with mice containing a conditional STAT3-knockout allele (STAT3lox). The gradual accumulation of ADM and PanIN and long latency for formation of invasive PDAC in the Pdx1-Cre; LSL-KRASG12D model makes it ideal for evaluating early stages of tumorigenesis. Pdx1-Cre; LSL-KRASG12D; STAT3lox/lox mice exhibited complete loss of P-STAT3 and total STAT3 in the pancreas (Supplementary Fig. S5A, B), indicating effective Cre-mediated recombination. Consistent with previous reports, the pancreas of Pdx1-Cre; STAT3lox/lox mice

developed normally, and these mice did not show any evident physiologic alterations (Fig. 4A). We isolated pancreata from Pdx1-Cre; LSL-KRASG12D; STAT3lox/lox mice or from Pdx1-Cre; LSL-KRASG12D; STAT3lox/+ controls at 12 weeks of age and quantified the extent of pancreatic lesions (see Methods). At this time point, control mice showed extensive ADM and PanIN formation (Fig. 4A), resulting in largely distorted pancreatic architecture. By contrast, in mice with STAT3 ablation, the majority of the pancreas had normal structure with only sporadic foci of ADM and PanIN. Correspondingly, the formation of ADM and PanIN was reduced 2.4-fold ($p=0.01$) and 6.6-fold ($p<0.001$), respectively, in Pdx1-Cre; KRASG12D; STAT3lox/lox mice, relative to controls (Figs. 4B, C). Thus, STAT3 plays a critical role in the robust formation of ADM and PanIN induced by oncogenic KRAS. While STAT3 ablation did not completely eliminate formation of these lesions, it led to a greatly attenuated ADM/PanIN phenotype.

Previous work has suggested a link between STAT3 and ADM. In a transgenic mouse model of ADM driven by persistent pancreatic expression of Pdx1, genetic inactivation of STAT3 can block ADM (20). Our data suggest that loss of STAT3 can also inhibit ADM in the more physiologically relevant setting of KRAS activation. The loss of polarized epithelium and reduced cell contacts associated with ADM

may create a permissive environment for further processes of cellular transformation. Therefore, it is possible that the involvement of STAT3 in KRAS-induced pancreatic tumorigenesis could be restricted to its role in the formation of these very early lesions. The associated reduction in PanINs could thus simply reflect decreased frequency of ADM precursors, whereas STAT3 maybe dispensable for continued pancreatic tumorigenesis once ADM has occurred. To begin to answer this question, we examined proliferation rates of ADM and PanIN lesions that formed in STAT3-null and control pancreata. Notably, STAT3 ablation resulted in significantly reduced levels of proliferation, as assessed by Ki67 staining, in both ADM and PanIN lesions (Figs. 5A–C), indicating a continued role for STAT3 in the proliferation and progression of early pancreatic lesions, even after ADM has occurred. An ongoing role for STAT3 in pancreatic tumorigenesis is consistent with the persistent expression of P-STAT3 observed at multiple stages of tumorigenesis, including PanINs and fully developed PDAC (Figs. 3A, B).

STAT3 is required for the progression to invasive PDAC

We next sought to determine the role of STAT3 in the progression to advanced PDAC. To this end, we isolated pancreatic ductal cells from 9 week-old Pdx1-Cre; LSL-KRASG12D mice. These cells are not tumorigenic upon orthotopic injection into recipient mice, whereas

shRNA-mediated inactivation of p53 enables these cells to rapidly progress to form invasive PDAC. To examine the effect of STAT3 loss on the tumorigenic potential of KRAS-shp53 ductal cells, we used two shRNA constructs targeting STAT3, which led to varying degrees of STAT3 knockdown and caused a marked decrease in the proliferation of KRAS-shp53 ductal cells, compared to control shRNA (Fig. 6A). When these cells were injected orthotopically, expression of shSTAT3 dramatically reduced PDAC formation compared to control shRNA, reducing the tumor volume from 2.9-fold (shSTAT3-1) to 11.5-fold (shSTAT3-2), consistent with the degree of STAT3 knockdown produced (Figs. 6B, C). The tumors that formed from shControl cells showed mainly features moderately-differentiated and poorly-differentiated PDAC (Fig. 6D, upper left panel), with only focal areas of PanINs. By contrast, the small tumors that form upon STAT3 knockdown showed a higher proportion of PanIN in addition to regions of moderately-differentiated PDAC (Fig. 6D, lower left panel). Immunofluorescence analysis confirmed that the shSTAT3 tumors lacked detectable STAT3 expression (Fig. 6D, middle panels). Notably, Ki-67 staining analysis of areas of invasive cancer showed that the shSTAT3 PDAC had a >3-fold reduction in proliferation rates ($p<0.001$) (Fig 6D, right panels and chart). Thus, reduction in STAT3 expression attenuates progression to invasive PDAC, and impairs the growth of the tumors that ultimately form. Collectively our studies

demonstrate that STAT3 is an important component of the molecular program driving PDAC progression and identify critical roles of this transcription factor at multiple stage of disease pathogenesis.

Discussion

PDAC carry extremely poor prognosis, and, in contrast to recent advances in several other common epithelial cancers, studies to date have not defined molecular features in PDAC patients that predict sensitivity to specific targeted therapies. Here, by systematic screening of >500 cancer cell lines—including 46 derived from PDAC—we identified a subset of PDAC cell lines with high sensitivity to JAK2 inhibition, and showed that this subset is characterized by activation of the gp130-STAT3 pathway. Importantly, we validated the functional role of STAT3 in PDAC pathogenesis in vivo. In keeping with the pronounced activation of STAT3 seen in ADM and PanIN in tissue specimens, genetic inactivation of STAT3 dramatically reduced both ADM and PanIN formation driven by oncogenic KRAS (Figs. 4A–C). Moreover, STAT3 inactivation blocked malignant progression to invasive PDAC despite concurrent knockdown of p53 in these cells (Figs. 6C, D). Thus, our data support a critical requirement for aberrant activation of STAT3 at multiple stages of PDAC initiation,

progression, and maintenance. Importantly, several JAK2 inhibitors are in advanced clinical development (41), and our studies suggest the potential of using levels of P-STAT3 and gp130 as biomarkers for patient selection in future clinical trials for PDAC using these compounds.

P-STAT3 is first detected in ADM (Fig. 3A), the earliest pre-neoplastic lesions arising in KRAS-driven PDAC models (40). Correspondingly, while STAT3 is completely dispensable for normal pancreatic development and function, its loss dramatically reduces formation of ADM induced by oncogenic KRAS (Fig. 4A, B). This requirement for STAT3 in KRAS-induced ADM is consistent with previous data demonstrating the importance of STAT3 for ADM induced by aberrant pancreatic expression of Pdx1, a homeobox transcription factor that controls the specification and expansion of early pancreatic progenitors in the embryo (20). In addition to facilitating ADM formation and ensuing development of PanIN, activated STAT3 has an ongoing role in sustaining PanIN proliferation and progression to PDAC, and in the viability of a subset of PDAC cell lines. The broad requirement for STAT3 at early stages of PDAC tumorigenesis and its more restricted role in established PDAC cell lines suggest that STAT3 may have temporally specific functions during tumor evolution.

STAT3 regulates several processes that potentially contribute to tumorigenesis, including subverting cellular differentiation programs, controlling energy metabolism, regulating an inflammatory transcriptional program, and promoting cellular survival (7,42–45). The early role of STAT3 in ADM driven either by oncogenic KRAS or by the aberrant expression of Pdx1, may reflect a requirement for STAT3 in developmental reprogramming as is observed in glioma (45,46), whereas, alternate processes may be operative in more advanced lesions that harbor additional gene mutations. Although additional investigation will be required to define functions of STAT3 in evolving PDAC, the marked inhibition of cell proliferation and survival upon STAT3 knockdown in KRAS-shp53 ductal cells and treatment of PDAC cells with the JAK2 inhibitor demonstrate a key cell autonomous role for JAK-STAT3 signaling.

STAT3 is activated by numerous growth factor and cytokine signaling pathways as well as by oncogenic RAS (7,34,43). Despite the prevalence of oncogenic KRAS mutations in human PDAC, they do not appear to contribute to STAT3 tyrosine phosphorylation in this setting since shRNAs targeting KRAS did not reduce P-STAT3 levels in PDAC cell lines (data not shown). Rather, our data demonstrate that high levels of P-STAT3 seen in ~40% of PDAC cell lines are due to

differential expression of the gp130 receptor. In particular, P-STAT3 and gp130 levels showed a close correlation, and gp130 blocking antibodies specifically extinguished STAT3 tyrosine phosphorylation in the subset of PDAC cell lines showing strong activation of the pathway. We also observed increased gp130 expression in human PDAC relative to normal pancreas. Gp130 is a component of the IL6 receptor complex, and consistent with the importance of this pathway, its ligands, LIF and IL6 were also prominently elevated in human PDAC tissues. The data in cell lines indicate an important role for autocrine signaling for STAT3 activation in established PDAC, however, our findings also suggest a potential mechanism linking inflammation with ADM and pancreatic tumor initiation. ADM is observed under conditions of chronic inflammation, such as chronic pancreatitis, and chronic pancreatitis is a risk factor for PDAC (47,48). It appears likely that release of cytokines, particularly members of the IL6 cytokine family, during inflammatory conditions may lead to activation of STAT3 and may cooperate with mutated KRAS to promote ADM and PanIN formation.

In summary, our findings in mouse models and human cell lines support the therapeutic targeting of STAT3 signaling in PDAC and indicate that JAK2 inhibitors may have utility in this cancer. Recent

clinical successes with targeted therapies directed at subsets of solid tumors harboring specific genetic or protein biomarkers, such as mutations in EGFR, ALK, or BRAF or amplification/overexpression of HER2 have created a paradigm for personalized approaches to cancer therapy (49). It is possible that P-STAT3 or IL6 cytokine family signaling could serve as biomarkers to guide similar approaches to applying therapies targeted against the STAT3 pathway in PDAC.

GRANT SUPPORT

R.B.C was supported by NIH training grant T32 CA071345. G.C. was supported by Fondazione Umberto Veronesi and Associazione Italiana per la ricerca sul Cancro. This work was support by grants to N.B. from the AACR-Pancreatic Cancer Action Network, Waxman Foundation for Cancer Research, NIH (NCI 2P01CA117969-06), and Dana-Farber/Harvard Cancer Center Gastrointestinal Cancer SPORE grant P50 CA127003 (to N.B. and J.A.E.)

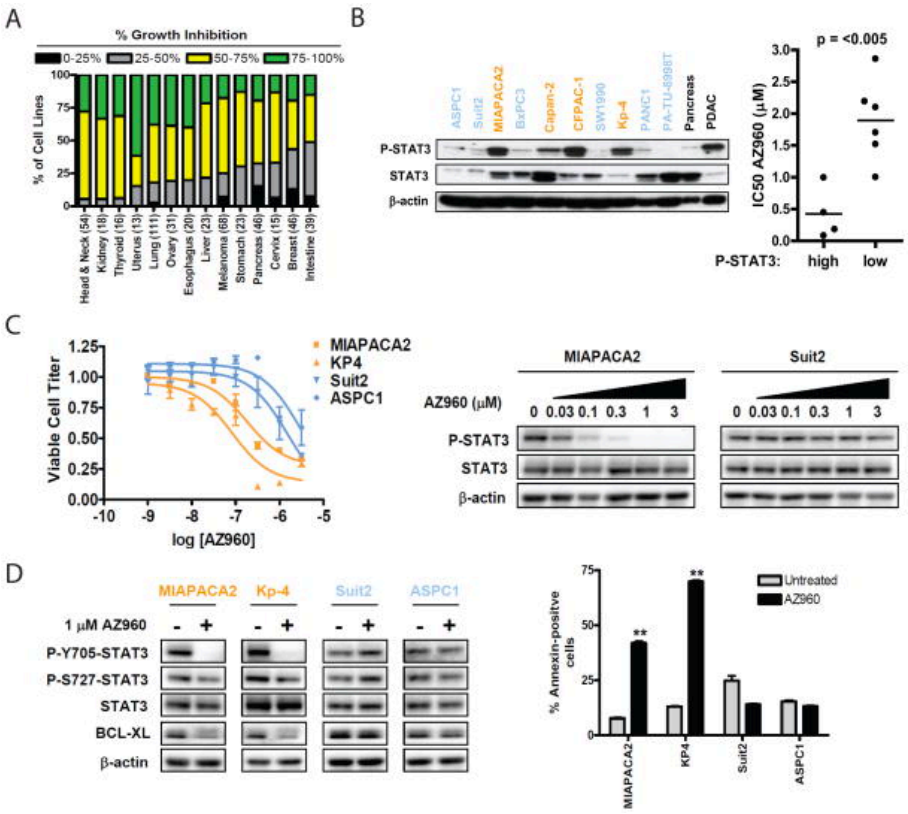

Figure 1 P-STAT3 levels predict sensitivity of PDAC cell lines to JAK2 inhibition

A, Analysis of the drug sensitivity profile of AZ960 (3μM) over a panel of >500 solid tumor cell lines based on tumor type (total number of cell lines in parenthesis). Bar color indicates percent growth inhibition relative to control. Bar height represents the percentage of cell lines of each tumor type showing the indicated degree of growth inhibition. B, left, western blot of P-STAT3 and total STAT3 levels in 10 PDAC cell lines, compared to normal pancreas and PDAC tissue. Right, comparison of the IC50 of AZ960 in PDAC cell lines with high vs. low P-STAT3 levels. Bar represents the mean IC50 value for each group. P-value is shown. C, left, PDAC cell lines with high (orange) or low (blue) P-STAT3 levels were treated in triplicate with the indicated concentrations of AZ960 for 72h. Viable cell titer was determined, and average values are shown relative to untreated controls for each cell line. Error bars represent SD for each measurement. Right, western blot of PDAC cell lines treated with the indicated concentrations of AZ960 for 24h. D, left, PDAC cell lines were treated in the presence or absence of 1μM AZ960 for 24h. Lysates were probed with the indicated antibodies. Right, PDAC cell lines were treated in the presence or absence of 1μM AZ960 for 72h. Percent apoptotic cells was determined by Annexin V staining (**p<0.01).

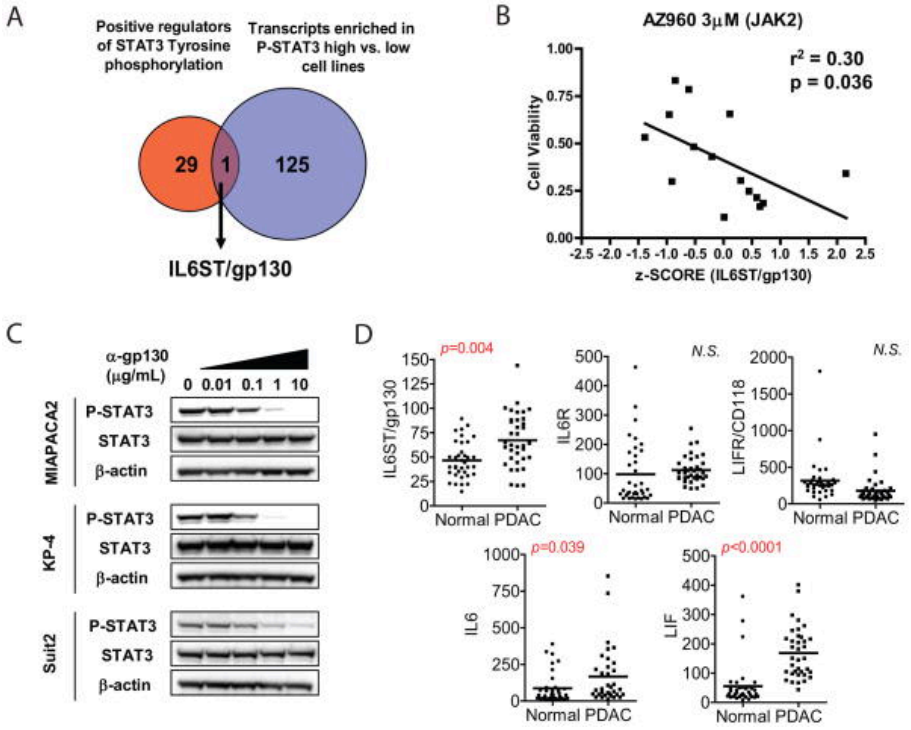

Figure 2. P-STAT3 is regulated by IL6 cytokine family signaling in PDAC cell lines A, Gene expression micorarray data from P-STAT3 high and low PDAC lines were analyzed to identify transcripts differentially enriched in P-STAT3 high cell lines. 126 transcripts found to be enriched in P-STAT3 high cell lines were cross-referenced with 30 positive regulators of STAT3 tyrosine phosphorylation identified by gene ontology search. Only one gene, IL6ST (encoding gp130) was present in both data sets. B, IL6ST transcript level z-score for 15 PDAC cell lines was correlated with drug sensitivity data to 3μM AZ960 from a large cell line repository drug screen. P value and r2 value are shown. C, PDAC cell lines were treated for 24h with increasing concentrations of gp130-neutralizing antibody. Cell lysates were probed with the indicated antibodies. D, Gene expression microarray data from 36 human PDACs and matched normal pancreas controls (normal) were analyzed for expression of IL6 cytokine family members. Bars represent mean of each group. P values are shown (N.S., not significant).

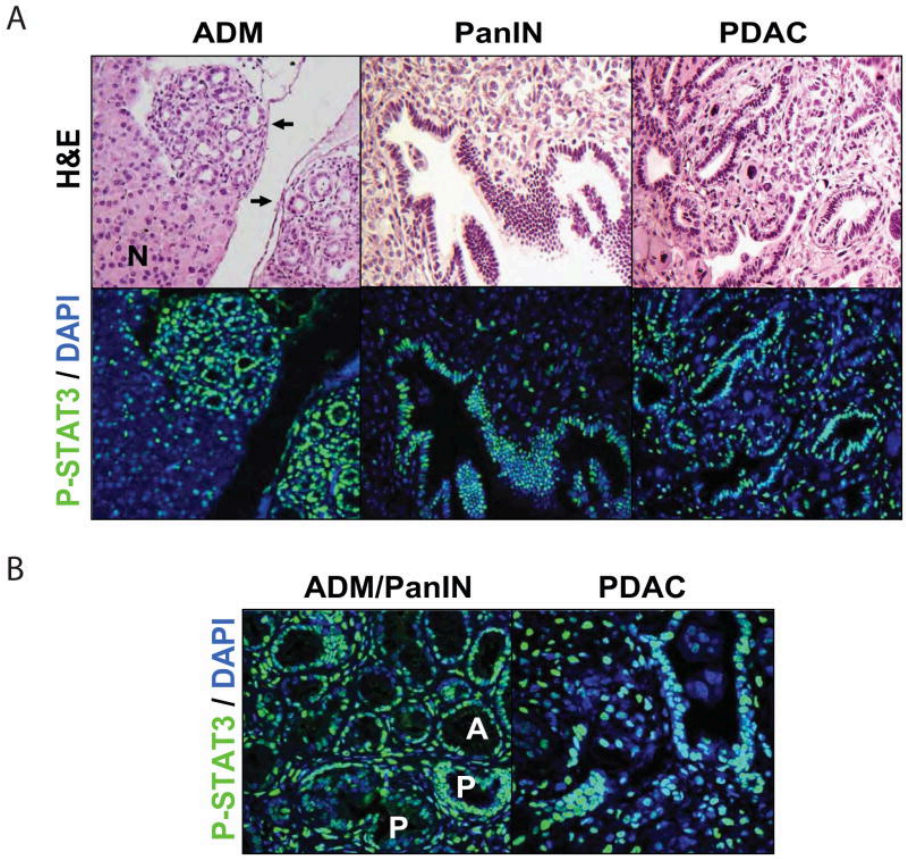

Figure 3. STAT3 is phosphorylated at multiple stages of pancreatic tumorigenesis

A, ADM and late-stage PanIN tissue from Pdx1-Cre; LSL-KRASG12D mice and PDAC tissue from Pdx1-Cre; LSL-KRASG12D; p53+/− mice were analyzed for the presence of P-STAT3 (green) by immunofluoresence with DAPI nuclear counterstain (blue). After image capture, slides were stained with hematoxylin and eosin (H&E). Arrows indicate regions of ADM. Normal pancreas is indicated by (N). B, higher magnification images of P-STAT3 staining (green) in ADM (upper half of image, A) or early-stage PanIN (lower half of image, P) lesions or in PDAC are shown.

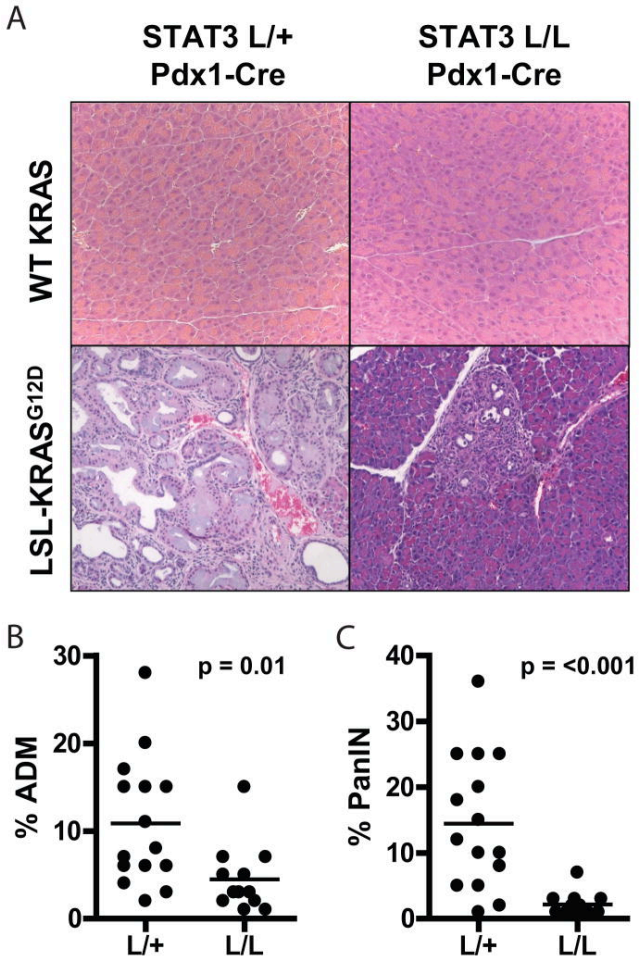

Figure 4. Loss of STAT3 decreases KRAS-induced ADM and PanIN formation

A, pancreatic tissue from 12 week-old Pdx1-Cre; STAT3lox/+ (L/+) or Pdx1-Cre; STAT3lox/lox (L/L) mice homozygous for wild-type KRAS alleles (upper panels) or heterozygous for the LSL-KRASG12D allele (lower panels) were harvested and stained with hematoxylin and eosin. B–C, the percent of each pancreas occupied by ADM (B) or PanIN (C) was calculated for each mouse. Each point represents a single mouse, and horizontal bars represent mean percentage for each group. P-values are shown.

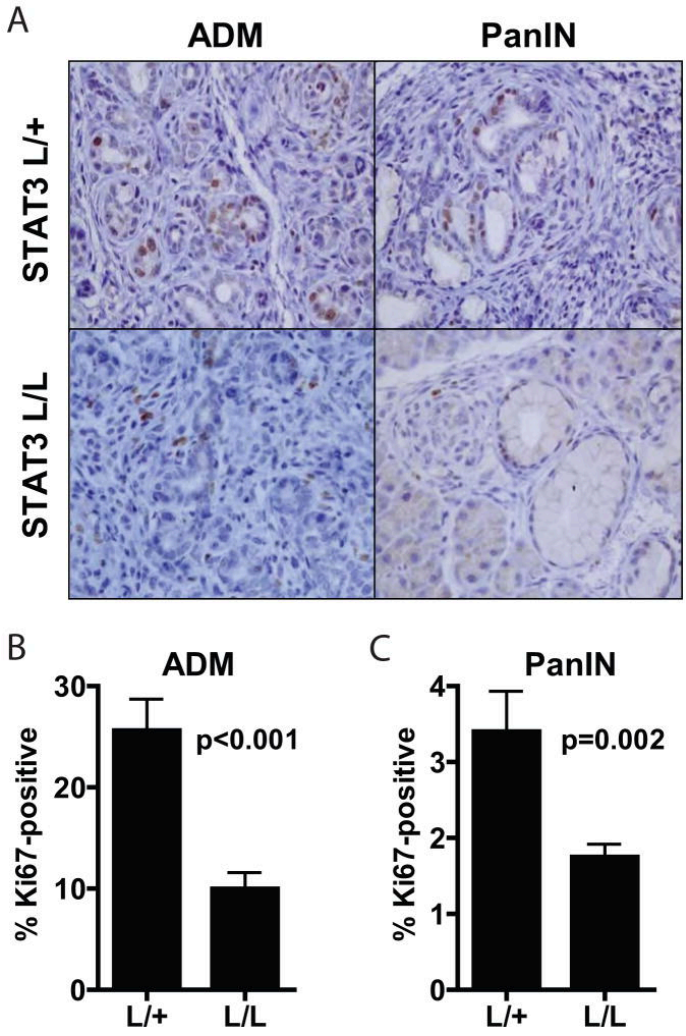

Figur 5. ADM and PanIN lesions that form in the absence of STAT3 show decreased proliferation

A, pancreatic tissue from 12 week-old *Pdx1-Cre; LSL-KRAS^{G12D}; STAT3$^{lox/+}$* (L/+) or *Pdx1-Cre; LSL-KRAS^{G12D}; STAT3$^{lox/lox}$* (L/L) mice was harvested and stained for Ki67. B-C, the percentage of Ki67-positive nuclei in ADM (B) or PanIN (C) lesions was calculated for each genotype, and mean percentage is shown. Error bars represent SD. P-values are shown.

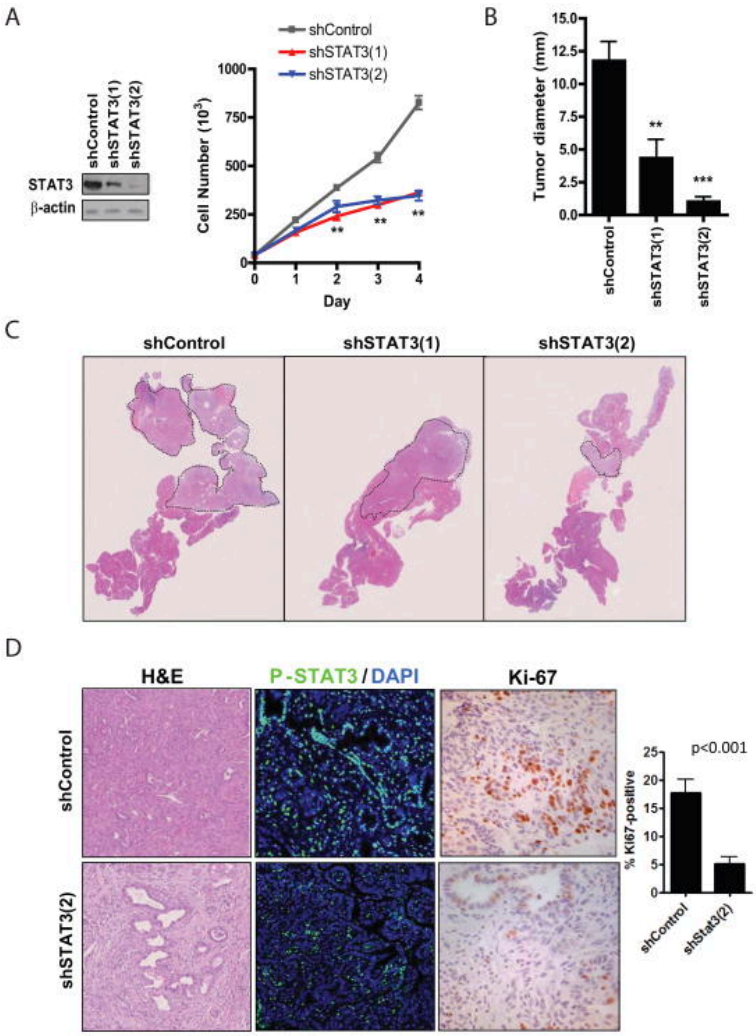

Figure 6. STAT3 knockdown prevents PDAC initiation in vivo

A, KRAS-shp53 ductal cells were infected with the indicated shRNAs and analyzed by western blot (left panel) and by cell counting. Measurements were performed in triplicate, and average values are shown (**p<0.001). Error bars represent SD. B, Equal numbers of KRAS-shp53 ductal cells infected with the indicated shRNAs were injected orthotopically into the pancreata of recipient mice. After 4 weeks, pancreatic tissue was harvested and the maximum tumor diameter was determined. Values represent the average tumor diameter for each group, and error bars represent SD (**p<0.01, ***p<0.001). C, upper, low magnification view of sectioned pancreas from representative mice harvested as in C. Dashed lines outline tumor tissue. D, Representative images of orthotopic tumors expressing shControl or shSTAT3(2) analyzed by H&E staining (Left, 200x),

immunofluorescence for P-STAT3 staining (Middle; green, P-STAT3, blue, DAPI nuclear counterstain), and immunohistochemical analysis of Ki-67 staining (Right, 400x). The percentage of Ki-67-positive nuclei represented in the graph; the great majority of Ki-67 staining was in the tumor epithelial cells, whereas only occasional stromal cells were Ki-67+.

References

1. Warshaw AL, Fernández-del Castillo C. Pancreatic carcinoma. N Engl J Med. 1992;326:455–65.

2. Hruban RH, van Mansfeld AD, Offerhaus GJ, van Weering DH, Allison DC, Goodman SN, et al. K-ras oncogene activation in adenocarcinoma of the human pancreas. A study of 82 carcinomas using a combination of mutant-enriched polymerase chain reaction analysis and allele-specific oligonucleotide hybridization. Am J Pathol. 1993;143:545–54.

3. Klimstra DS, Longnecker DS. K-ras mutations in pancreatic ductal proliferative lesions. Am J Pathol. 1994;145:1547–50.

4. Moskaluk CA, Hruban RH, Kern SE. p16 and K-ras gene mutations in the intraductal precursors of human pancreatic adenocarcinoma. Cancer Res. 1997;57:2140–3.

5. Rozenblum E, Schutte M, Goggins M, Hahn SA, Panzer S, Zahurak M, et al. Tumor-suppressive pathways in pancreatic carcinoma. Cancer Res. 1997 May 1;57(9):1731–4.

6. Hruban RH, Goggins M, Parsons J, Kern SE. Progression model for pancreatic cancer. Clin Cancer Res. 2000;6:2969–72.

7. Frank DA. STAT3 as a central mediator of neoplastic cellular transformation. Cancer Lett. 2007;251:199–210.

8. Shuai K, Stark GR, Kerr IM, Darnell JE., Jr A single phosphotyrosine residue of Stat91 required for gene activation by interferon-gamma. Science. 1993;261:1744–6.

9. Shuai K, Horvath CM, Huang LH, Qureshi SA, Cowburn D, Darnell JE., Jr Interferon activation of the transcription factor Stat91 involves dimerization through SH2-phosphotyrosyl peptide interactions. Cell. 1994;76:821–8.

10. Darnell JE, Jr, Kerr IM, Stark GR. Jak-STAT pathways and transcriptional activation in response to IFNs and other extracellular signaling proteins. Science. 1994;264:1415–21.

11. Zhong Z, Wen Z, Darnell JE., Jr Stat3: a STAT family member activated by tyrosine phosphorylation in response to epidermal growth factor and interleukin-6. Science. 1994;264:95–8.

12. Cao X, Tay A, Guy GR, Tan YH. Activation and association of Stat3 with Src in v-Src-transformed cell lines. Mol Cell Biol. 1996;16:1595–603.

13. Bromberg J, Darnell JE., Jr The role of STATs in transcriptional control and their impact on cellular function. Oncogene. 2000;19:2468–73.

14. Bao S, Tang F, Li X, Hayashi K, Gillich A, Lao K, Surani MA. Epigenetic reversion of post-implantation epiblast to pluripotent embryonic stem cells. Nature. 2009;461:1292–5.

15. Chan KS, Sano S, Kiguchi K, Anders J, Komazawa N, Takeda J, DiGiovanni J. Disruption of Stat3 reveals a critical role in both the initiation and the promotion stages of epithelial carcinogenesis. J Clin Invest. 2004;114:720–8.

16. Jenkins BJ, Grail D, Nheu T, Najdovska M, Wang B, Waring P, et al. Hyperactivation of Stat3 in gp130 mutant mice promotes gastric hyperproliferation and desensitizes TGF-beta signaling. Nat Med. 2005;11:845–52.

17. Scholz A, Heinze S, Detjen KM, Peters M, Welzel M, Hauff P, et al. Activated signal transducer and activator of transcription 3 (STAT3) supports the malignant phenotype of human pancreatic cancer. Gastroenterology. 2003;125:891–905.

18. Toyonaga T, Nakano K, Nagano M, Zhao G, Yamaguchi K, Kuroki S, et al. Blockade of constitutively activated Janus kinase/signal transducer and activator of transcription-3 pathway inhibits growth of human pancreatic cancer. Cancer Lett. 2003;201:107–16.

19. Lee JY, Hennighausen L. The transcription factor Stat3 is dispensable for pancreatic beta-cell development and function. Biochem Biophys Res Commun. 2005;334:764–8.

20. Miyatsuka T, Kaneto H, Shiraiwa T, Matsuoka TA, Yamamoto K, Kato K, et al. Persistent expression of PDX-1 in the pancreas causes acinar-to-ductal metaplasia through Stat3 activation. Genes Dev. 2006;20:1435–40.

21. Wei D, Le X, Zheng L, Wang L, Frey JA, Gao AC, Peng Z, Huang S, Xiong HQ, Abbruzzese JL, Xie K. Stat3 activation regulates the expression of vascular endothelial growth factor and human pancreatic cancer angiogenesis and metastasis. Oncogene. 2003;22:319–29.

22. Jaganathan S, Yue P, Turkson J. Enhanced sensitivity of pancreatic cancer cells to concurrent inhibition of aberrant signal transducer and activator of transcription 3 and epidermal growth factor receptor or Src. J Pharmacol Exp Ther. 2010;333:373–81.

23. Gu G, Dubauskaite J, Melton DA. Direct evidence for the pancreatic lineage: NGN3+ cells are islet progenitors and are distinct from duct progenitors. Development. 2002;129:2447–57.

24. Hingorani SR, Petricoin EF, Maitra A, Rajapakse V, King C, Jacobetz MA, et al. Preinvasive and invasive ductal pancreatic cancer and its early detection in the mouse. Cancer Cell. 2003 Dec;4(6):437–50.

25. Lee CK, Raz R, Gimeno R, Gertner R, Wistinghausen B, Takeshita K, et al. STAT3 is a negative regulator of granulopoiesis but is not required for G-CSF-dependent differentiation. Immunity. 2002;17:63–72.

26. Agbunag C, Lee KE, Buontempo S, Bar-Sagi D. Pancreatic duct epithelial cell isolation and cultivation in two-dimensional and three-dimensional culture systems. Methods Enzymol. 2006;407:703–10.

27. Dickins RA, Hemann MT, Zilfou JT, Simpson DR, Ibarra I, Hannon GJ, et al. Probing tumor phenotypes using stable and regulated synthetic microRNA precursors. Nat Genet. 2005;37:1289–95.

28. Mohammad RM, Al-Katib A, Pettit GR, Vaitkevicius VK, Joshi U, Adsay V, et al. An orthotopic model of human pancreatic cancer in severe combined immunodeficient mice: potential application for preclinical studies. Clin Cancer Res. 1998;4:887–94.

29. Gozgit JM, Bebernitz G, Patil P, Ye M, Parmentier J, Wu J, et al. Effects of the JAK2 inhibitor, AZ960, on Pim/BAD/BCL-xL survival signaling in the human JAK2 V617F cell line SET-2. J Biol Chem. 2008;283:32334–43.

30. McDermott U, Sharma SV, Dowell L, Greninger P, Montagut C, Lamb J, et al. Identification of genotype-correlated sensitivity to selective kinase inhibitors by using high-throughput tumor cell line profiling. Proc Natl Acad Sci U S A. 2007;104:19936–41.

31. Wen Z, Darnell JE., Jr Mapping of Stat3 serine phosphorylation to a single residue (727) and evidence that serine phosphorylation has no influence on DNA binding of Stat1 and Stat3. Nucleic Acids Res. 1997;25:2062–7.

32. Zhang X, Blenis J, Li HC, Schindler C, Chen-Kiang S. Requirement of serine phosphorylation for formation of STAT-promoter complexes. Science. 1995;267:1990–4.

33. Taga T, Narazaki M, Yasukawa K, Saito T, Miki D, Hamaguchi M, et al. Functional inhibition of hematopoietic and neurotrophic cytokines by blocking the interleukin 6 signal transducer gp130. Proc Natl Acad Sci U S A. 1992;89:10998–1001.

34. Kishimoto T, Akira S, Narazaki M, Taga T. Interleukin-6 family of cytokines and gp130. Blood. 1995;86:1243–54.

35. Kitamura T, Tange T, Terasawa T, Chiba S, Kuwaki T, Miyagawa K, et al. Establishment and characterization of a unique human cell line that proliferates dependently on GM-CSF, IL-3, or erythropoietin. J Cell Physiol. 1989;140:323–34.

36. Aguirre AJ, Bardeesy N, Sinha M, Lopez L, Tuveson DA, Horner J, et al. Activated Kras and Ink4a/Arf deficiency cooperate to produce metastatic pancreatic ductal adenocarcinoma. Genes Dev. 2003;17:3112–26.

37. Hingorani SR, Wang L, Multani AS, Combs C, Deramaudt TB, Hruban RH, et al. Trp53R172H and KrasG12D cooperate to promote chromosomal instability and widely metastatic pancreatic ductal adenocarcinoma in mice. Cancer Cell. 2005 May;7(5):469–83.

38. Bardeesy N, Aguirre AJ, Chu GC, Cheng KH, Lopez LV, Hezel AF, et al. Both p16(Ink4a) and the p19(Arf)-p53 pathway constrain progression of pancreatic adenocarcinoma in the mouse. Proc Natl Acad Sci U S A. 2006;103:5947–52.

39. Shi C, Hong SM, Lim P, Kamiyama H, Khan M, Anders RA, et al. KRAS2 mutations in human pancreatic acinar-ductal metaplastic lesions are limited to those with PanIN: implications for the human pancreatic cancer cell of origin. Mol Cancer Res. 2009;7:230–6.

40. Zhu L, Shi G, Schmidt CM, Hruban RH, Konieczny SF. Acinar cells contribute to the molecular heterogeneity of pancreatic intraepithelial neoplasia. Am J Pathol. 2007;171:263–73.

41. Hedvat M, Huszar D, Herrmann A, Gozgit JM, Schroeder A, Sheehy A, et al. The JAK2 inhibitor AZD1480 potently blocks Stat3 signaling and oncogenesis in solid tumors. Cancer Cell. 2009;16:487–97.

42. Iliopoulos D, Hirsch HA, Struhl K. An epigenetic switch involving NF-kappaB, Lin28, Let-7 MicroRNA, and IL6 links inflammation to cell transformation. Cell. 2009;139:693–706.

43. Gough DJ, Corlett A, Schlessinger K, Wegrzyn J, Larner AC, Levy DE. Mitochondrial STAT3 supports Ras-dependent oncogenic transformation. Science. 2009;324:1713–6.

44. Wegrzyn J, Potla R, Chwae YJ, Sepuri NB, Zhang Q, Koeck T, et al. Function of mitochondrial Stat3 in cellular respiration. Science. 2009;323:793–7.

45. Sherry MM, Reeves A, Wu JK, Cochran BH. STAT3 is required for proliferation and maintenance of multipotency in glioblastoma stem cells. Stem Cells. 2009;27:2383–92.

46. Carro MS, Lim WK, Alvarez MJ, Bollo RJ, Zhao X, Snyder EY, Sulman EP, Anne SL, Doetsch F, Colman H, Lasorella A, Aldape K, Califano A, Iavarone A. The transcriptional network for mesenchymal transformation of brain tumours. Nature. 2010;463:318–25.

47. Lowenfels AB, Maisonneuve P, DiMagno EP, Elitsur Y, Gates LK, Jr, Perrault J, et al. Hereditary pancreatitis and the risk of pancreatic cancer. International Hereditary Pancreatitis Study Group. J Natl Cancer Inst. 1997;89:442–6.

48. Hezel AF, Kimmelman AC, Stanger BZ, Bardeesy N, Depinho RA. Genetics and biology of pancreatic ductal adenocarcinoma. Genes Dev. 2006;20:1218–49.

49. McDermott U, Settleman J. Personalized cancer therapy with selective kinase inhibitors: an emerging paradigm in medical oncology. J Clin Oncol. 2009;27:5650–9.

Supplementary Materials and Methods

Reagents and Antibodies

AZ960 was purchased from Symansis. Neutralizing monoclonal antibody to gp130 was purchased from R&D Systems. For western blotting, antibodies to Phospho-STAT3 (Tyr705), Phospho-STAT3 (Ser727), STAT3, gp130, and BCL-XL were purchased from Cell Signaling. Antibody to b-actin was purchased from Sigma. Antibody to GAPDH was purchased from Chemicon.

Western Blot analysis

Western blotting was performed using standard methods. Cells were washed with cold PBS and lysed in the following lysis buffer: 20 mM Tris pH 7.4, 150 mM NaCl, 1% Nonidet P-40, 10% glycerol, 1 mM EDTA, 1 mM EGTA, 5 mM sodium pyrophosphate, 50 mM NaF, 10 nM b–glycerophosphate, 1 mM sodium vanadate, 0.5 mM DTT, 4 mg/mL leupeptin, 4 mg/mL pepstatin, 4 mg/mL aprotinin, 1 mM phenylmethylsulfonyl fluoride. Lysates were centrifuged at 16,000 x *g* for 5 min at 4°C. Pancreatic tissues (100-200mg) were minced by using a homogenizer, but otherwise processed as above. Protein concentrations were determined by BCA assay (Thermo Scientific). Proteins were resolved by SDS-PAGE and transferred to a

polyvinylidene difluoride membrane (Hybond-P, Amersham). Immunoblotting was performed per antibody manufacturer's specifications.

Determination of Viable Cell Titer

Cells were seeded at 2,000 cells per well of a 96-well plate. After overnight incubation, the cells were treated in triplicate with serial dilutions of each drug for 72h. Viable cell titer relative to untreated cells was determined using Cell Titer Glo assay (Promega) according to the manufacturer's protocol using and read on a Centro LB 960 microplate luminometer (Berthold Technologies).

Annexin V Apoptosis Assays

Cells were seeded at ~30 to 40% confluence in 6 cm plates. After overnight incubation, media was aspirated and replaced with media with or without various concentrations of indicated drugs. After 72h, media was collected. Cells were washed with PBS and trypsinized. PBS wash and trypsinized cells were added to the collected media in a single tube. Cells were pelleted, washed once with PBS and resuspended in Annexin binding buffer (BD Biosciences) at ~1 x 10^6 cells/mL. Cells were stained with propidium iodide (BD Biosciences) and Annexin V Cy5 (Biovision) according to the manufacturer's protocol and assayed on a LSRII flow cytometer (BD Biosciences).

Gene Expression Microarray and Copy Number Analysis

Human PDAC cell line gene expression microarray data was obtained from the Broad Institute Sanger Cell Line Project (1). To identify transcripts enriched in PDAC cell lines with high P-STAT3 levels, gene expression data for 4 high P-STAT3 cell lines (MIAPACA2, KP-4, CFPAC-1, Capan-2) and 3 low P-STAT3 cell lines (BxPC3, SW1990, ASPC1) were analyzed. For each probe, the average Z-score for high P-STAT3 cell lines was compared to that of low P-STAT3 cell lines, and genes corresponding to probes for which the z-score was significantly higher ($p<0.01$) in high P-STAT3 were identified. This gene list was cross-referenced with a list of positive regulators of STAT3 tyrosine phosphorylation identified by gene ontology search (amigo.geneontology.org) to identify genes existing in both datasets. Gene expression data for human normal pancreas and PDAC were obtained from the Gene Expression Omnibus (GEO) Database (2). Coexpression of candidate transcripts with IL6ST in PDAC cell lines was assessed by Pearson correlation analysis. IL6ST copy number data for PDAC cell lines was obtained from the Sanger Institute Cancer Genome Project SNP database (3).

Cell Line Drug Screen Data Analysis

Drug sensitivity data from over 500 solid tumor cell lines were obtained from the cell line repository drug screen database of the Massachusetts General Hospital Center for Molecular Therapeutics (4). Correlation of drug sensitivity with IL6ST transcript level was performed for PDAC cell lines with available gene expression microarray data. For each cell line, and average z-score of all five

IL6ST probes present in the microarray data was correlated with the cell viability (relative to untreated control) of each cell line after treatment with the indicated concentrations of inhibitors.

Immunofluorescence and Immunohistochemistry

Samples were fixed in 10% formalin and embedded in paraffin. After deparaffinization slides are washed with 9.83% NaCl for 3 min followed by a PBS wash and a wash in distilled water for 5min. Heat induced antigen retrieval was performed with pressure cooker (2100 Retriever, PickCell Laboratories B.V.) and R-Buffer A (pH6.0, Electron Microscopy Sciences). Sections were incubated with 2% H_2O_2 in Methanol for 15 minutes for endogenous peroxidase quenching, washed and blocked for non specific binding in 1% BSA in PBS-triton 0.3% v/v (PBST) for 1 hour. Subsequently, sections were sequentially incubated with primary phospho-Stat3 (Tyr705) antibody (#9145, Cell Signaling) at 1:100 dilution for 1 hour, secondary peroxidase goat anti-rabbit IgG antibody (Vector) at 1:250 dilution for 1 hour and Tyramide Signal Amplification (TSA) Fluorescein System (Perkin Elmer, Cat.: NEL701A) according to kit manual. Slides were mounted with Vectashield mounting medium with DAPI (Vector), photographed with Nikon C2 Confocal Microscope system and subsequently stained with Hematoxylin and Eosin. Ki67 staining was performed as previously described (5). Quantification of Ki67 staining in ADM and PanIN was performed by scoring the nuclei of cells from each lesion type found in a minimum of ten high-powered fields.

Quantification was performed on pancreata from a minimum of three animals in each experimental cohort.

Cell Proliferation Assays

PanIN-derived cells infected with shStat3(1), shStat3(2) and shControl were plated at $4x10^4$ cells/well, in twelve well plates and there were passaged daily in 1:2 ratio. Cells were counted with an automatic cell counter (Countess, Automated Cell Counter; Invitrogen) according to the instructions of the manufacturer. The graphs show the cumulative cells number upon cell passaging for the indicated period of time.

Orthotopic injection and Histological characterization

SCID mice (C3SnSmn.CB17-*Prkdc*^{scid}/J, Jackson Lab) were subjected to general anesthesia with IP Avertin a (0.5mg/g) and subcutaneous Marcaine (0.1ml/25g mouse of 0.025% solution) analgesia according to MGH SRAC policies. Orthotopic injections were performed as previously described (6). Briefly, a left lateral laparatomy was performed and spleen and distal pancreas were mobilized. $2x10^4$ PanIN cells (viability >90%) were suspended in 50ml of Duct Media (7), mixed with 50ml of Matrigel (BD Biosciences), and injected into the pancreas. The abdominal incision was closed using silk suture 3/0 (Ethicon) for the peritoneum and surgical staples for the skin. After 4 weeks mice were sacrificed, and whole pancreas was carefully sectioned with a surgical blade and the longest nodule diameter annotated. Experiments were conducted at least in triplicate for each

condition. H&E slides were analyzed with LEICA DM1000A microscope and whole mount scanning performed with Nanozoomer 2.0 R-S (Hamamatsu).

shRNA and Lentiviral Infections

shRNA constructs in the pLKO.1 lentiviral vector with the following target sequences were used.

Mouse:

shSTAT3(1) (TRCN0000071454), 5'-CGACTTTGATTTCAACTACAA-3'

shSTAT3(2) (TRCN0000071456), 5'-CCTGAGTTGAATTATCAGCTT-3'

shControl 5'-GCAAGCTGACCCTGAAGTTCAT-3'.

Human:

shSTAT3(4) (TRCN0000020842), 5'- GCACAATCTACGAAGAATCAA-3'

shSTAT3(5) (TRCN0000020843), 5'- GCAAAGAATCACATGCCACTT-3'

shGFP 5'-GCAAGCTGACCCTGAAGTTCAT-3'

Viral particles were made by transfection of 293T cells with a three plasmid system as previously described (8). Target cells were incubated with lentiviruses in the presence of 8 mg/mL polybrene. The following morning, lentivirus-containing media was replaced with fresh media. Two days after infection, puromycin (2 mg/mL) was added for 3 days to eliminate uninfected cells.

Determination of IC50 and statistical analysis

Statistical analyses were performed using a two-tailed student's t-test (Figs. 1B, 1D, 2A, 4B-C, 5B-C, S1B) or ANOVA with Bonferroni's post-test (Figs. 2D, 6B-C). R^2 and p values determined by linear

regression analysis were made using GraphPad Prism software (Figs. 2B, S3). IC50 values were calculated using GraphPad Prism software.

References

1.) Broad Institute Sanger Cell Line Project. Available from: http://www.broadinstitute.org/cgi-bin/cancer/publications/pub_paper.cgi?mode=view&paper_id=189

2.) Edgar R, Domrachev M, Lash AE. Gene Expression Omnibus: NCBI gene expression and hybridization array data repository. Nucleic Acids Res 2002;30:207-10.

3.) Sanger Institute Cancer Genome Project SNP database. Available from: www.sanger.ac.uk/genetics/CGP

4.) McDermott U, Sharma SV, Dowell L, Greninger P, Montagut C, Lamb J, et al. Identification of genotype-correlated sensitivity to selective kinase inhibitors by using high-throughput tumor cell line profiling. Proc Natl Acad Sci U S A 2007;104:19936-41.

5.) Zhou D, Conrad C, Xia F, Park JS, Payer B, Yin Y, et al. Mst1 and Mst2 maintain hepatocyte quiescence and suppress hepatocellular carcinoma development through inactivation of the Yap1 oncogene. Cancer Cell 2009;16:425-38.

6.) Mohammad RM, Al-Katib A, Pettit GR, Vaitkevicius VK, Joshi U, Adsay V, et al. An orthotopic model of human pancreatic cancer in severe combined immunodeficient mice: potential

application for preclinical studies. Clin Cancer Res 1998;4:887-94.

7.) Agbunag C, Lee KE, Buontempo S, Bar-Sagi D. Pancreatic duct epithelial cell isolation and cultivation in two-dimensional and three-dimensional culture systems. Methods Enzymol 2006;407:703-10.

8.) Moffat J, Grueneberg DA, Yang X, Kim SY, Kloepfer AM, Hinkle G, et al. A lentiviral RNAi library for human and mouse genes applied to an arrayed viral high-content screen. Cell 2006;124:1283-98.

Supplemental Figure Legends

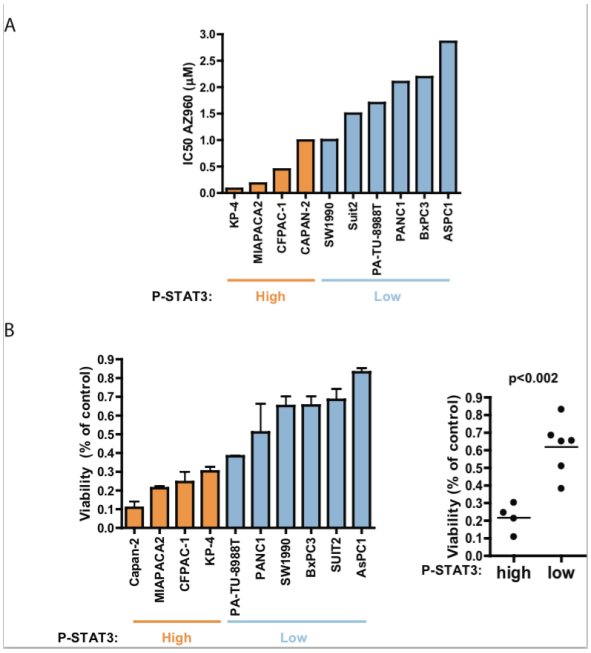

Fig. S1: Increased sensitivity of PDAC cell lines with high P-STAT3 to AZ960. A, Individual IC50 values for AZ960 in PDAC cell lines from Fig. 1B. Cell lines were cultured in increasing concentrations of AZ960 for 72h. Viable cell titer was determined, and IC50s were calculated as in Materials and Methods. B, left, individual cell viability determinations after 72h treatment with 3μM AZ960 for PDAC cell lines from Fig. 1B obtained from a large cell line repository screen. Values are shown relative to untreated control. Error bars represent SD. Right, comparison cell viability measurements after treatment with 3μM AZ960 in PDAC cell lines with high vs. low P-STAT3 levels. Bar represents the mean for each group. P-value is shown.

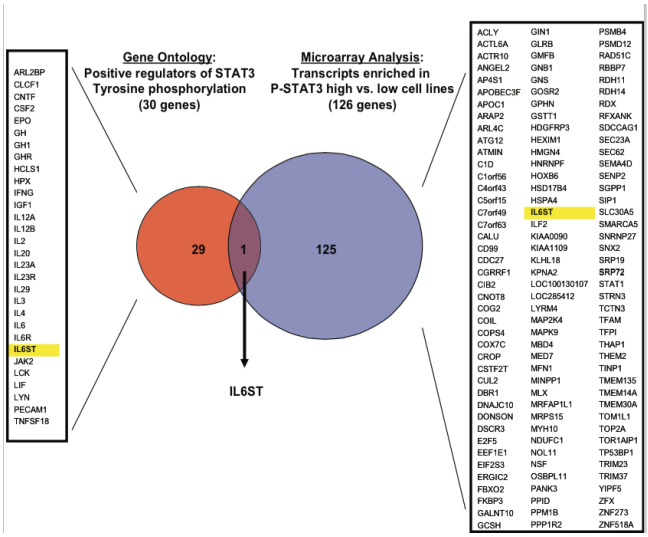

Fig. S2: IL6ST is a positive regulator of STAT3 tyrosine phosphorylation with increased transcript levels in PDAC cell lines with high P-STAT3 levels. The individual genes (as in Fig. 2A) identified as positive regulators of STAT3 tyrosine phosphorylation by gene ontology search (left, red) and the individual transcripts fount to be enriched in PDAC cell lines with high P-STAT3 levels (blue, right) are shown. IL6ST (highlighted in yellow) was the only gene identified in both gene sets.

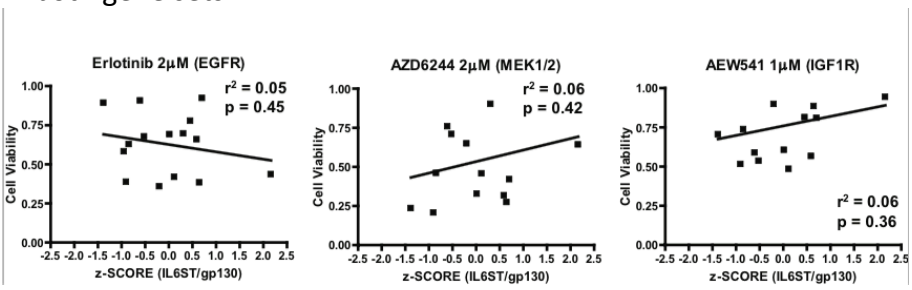

Fig. S3: IL6ST transcript level does not correlate with sensitivity of PDAC to inhibitors of EGFR, MEK1/2, and IGF1R. IL6ST transcript level z-score for PDAC cell lines was correlated with drug sensitivity data to various inhibitors (as in Fig. 2B) from a large cell line repository drug screen of >500 solid tumor cell lines. Each inhibitor, the concentration tested, the P value, and r2 value are shown.

A

Cell Line	IL6ST z-SCORE	IL6ST Copy #
PANC-03-27	2.162	4
PSN1	0.781	4
PANC-10-05	0.707	2
HUPT3	0.649	2
MIAPACA2	0.594	4
CFPAC1	0.456	4
KP4	0.310	4
BxPC3	0.119	2
Capan-2	0.0188	4
PANC-08-13	-0.197	2
YAPC	-0.519	4
CAPAN-1	-0.603	2
ASPC1	-0.843	3
HUPT4	-0.902	3
SW1990	-0.948	3
HPAF-II	-1.380	3

B

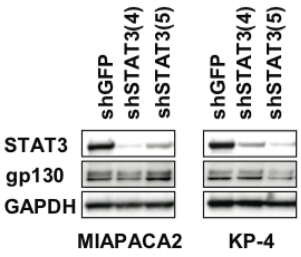

C

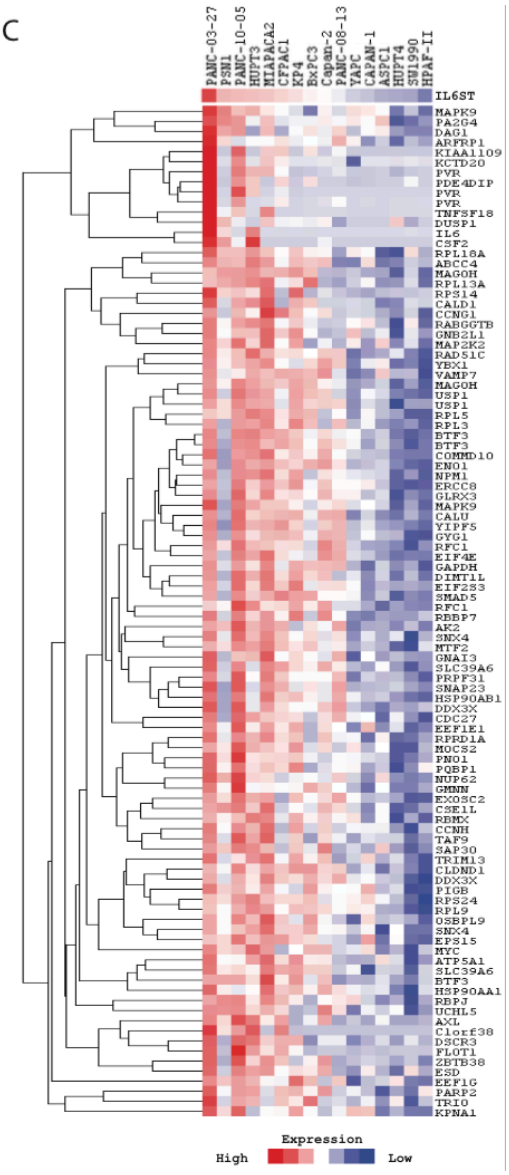

Fig. S4: Potential mechanisms of IL6ST/gp130 upregulation in PDAC cell lines. A, IL6ST transcript level does not correlate with IL6ST gene copy number. IL6ST copy number of PDAC cell lines as determined by SNP analysis compared with IL6ST transcript expression (z-SCORE). No focal amplification of IL6ST was observed. B, STAT3 knockdown does not markedly affect gp130 levels. P-STAT3 high PDAC cell lines MIAPACA2 and KP-4 were infected with shGFP or shRNA targeted against STAT3. After puromycin selection, cells were placed in media

with 5% FBS for 24h prior to lysis. Lysates were probed with the indicated antibodies. C, Potential regulators of IL6ST/gp130 expression. The 100 transcript probes showing the highest degree of coexpression with IL6ST as determined by Pearson correlation in a panel of PDAC cell lines.

A

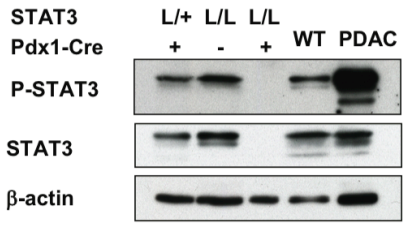

B

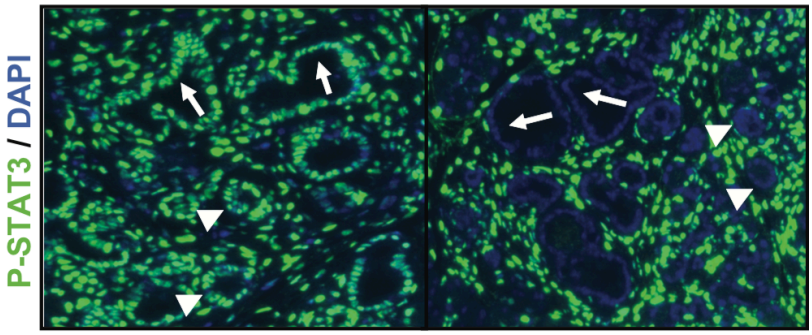

Fig. S5: Lack of STAT3 protein expression in the pancreas of Pdx1-Cre; STAT3L/L mice. A, Whole pancreas was isolated from 6 week old mice of the indicated genotypes. PDAC tissue was obtained from Pdx1-Cre; LSL-$KRAS^{G12D}$; $p53^{+/-}$ mice. Lysates were probed with the indicated antibodies. B, Pancreata from 12 week old Pdx1-Cre; LSL-$KRAS^{G12D}$; $STAT3^{lox/+}$ (STAT3 L/+) or Pdx1-Cre; LSL-$KRAS^{G12D}$; $STAT3^{lox/lox}$ (STAT3 L/L) mice were analyzed for the presence of P-STAT3 (green) by immunofluorescence with DAPI nuclear counterstain (blue). Nuclear P-STAT3 staining is absent from ADM (arrowheads) or PanIN (arrows) lesions that arise in the absence of STAT3 (STAT3 L/L), while P-STAT3 staining is still detected in the surrounding stroma. By contrast, in STAT3 L/+ mice, P-STAT3 staining is detected in ADM and PanIN, as well as in the surrounding stroma

Combined MEK and PI3K inhibition in a mouse model of pancreatic cancer

Brinda Alagesan[1*], Gianmarco Contino[1*], Alex Guimaraes[2,6], Ryan B. Corcoran[1,5], Vikram Deshpande[3,7], Gregory R. Wojtkiewicz[2], Aram F. Hezel[1,5], Kwok-Kin Wong[4,5], Massimo Loda[4,6,8], Ralph Weissleder[2,6], Cyril Benes[1,5], Jeffrey Engelman[1,5], Nabeel Bardeesy[1,5]

[1]Cancer Center, [2]Center for Molecular Imaging Research, and [3]Department of Pathology, Massachusetts General Hospital, Boston, MA 02114; [4]Department of Medical Oncology, Dana-Farber Cancer Institute, Boston MA 02215; and Departments of [5]Medicine, [6]Radiology and [7]Pathology, Harvard Medical School; [8]Department of Pathology, Brigham and Women's Hospital, Boston, MA 02115.

*these authors contributed equally

Key Words: Pancreatic cancer, MEK, PI3K, KRAS, high-throughput screens, Genetically engineered mouse models

TRANSLATIONAL RELEVANCE: Our results support the potential efficacy of combined MEK/PI3K inhibition in PDAC. MEK inhibitors were the most selectively active agents against PDAC cell lines in a high-throughput screen of 50 clinically relevant drugs in >500 human cancer cell lines. In combination with PI3K inhibitors, AZD-6244 is effective in promoting apoptosis in PDAC lines, and acted combinatorially with PI3K inhibitors in suppressing tumor initiation and progression in a genetically engineered mouse model of PDAC. Although the combination did not produce durable responses, our findings suggest that combined targeting of MEK and PI3K may be beneficial as a second-line therapy for PDAC patients.

ABSTRACT

Purpose: Improved therapeutic approaches are needed for the treatment of pancreatic ductal adenocarcinoma (PDAC). As dual MEK and PI3K inhibition is presently being employed in clinical trials for PDAC patients, we sought to test the efficacy of combined targeting of these pathways in PDAC using both *in vitro* drug screens and genetically engineered mouse models (GEMMs).

Experimental Design: We performed high-throughput screening of >500 human cancer cell lines (including 46 PDAC lines), for sensitivity to 50 clinically-relevant compounds, including MEK and PI3K inhibitors. We tested the top hit in the screen, the MEK1/2 inhibitor, AZD-6244, for efficacy alone or in combination with the PI3K inhibitors, BKM-120 or GDC-0941, in a $KRAS^{G12D}$-driven GEMM that recapitulates the histopathogenesis of human PDAC.

Results: In vitro screens revealed that PDAC cell lines are relatively resistant to single-agent therapies. The response profile to the MEK1/2 inhibitor, AZD-6244, was an outlier, showing the highest selective efficacy in PDAC. While MEK inhibition alone was mainly cytostatic, apoptosis was induced when combined with PI3K inhibitors (BKM-120 or GDC-0941). When tested in a PDAC GEMM and compared to the single agents or vehicle controls, the combination delayed tumor formation in the setting of prevention and extended survival when used to treat advanced tumors, although no durable responses were observed.

Conclusions: Our studies point to important contributions of MEK and PI3K signaling to PDAC pathogenesis and suggest that dual targeting of these pathways may provide benefit in some PDAC patients.

INTRODUCTION

Pancreatic ductal adenocarcinoma (PDAC) is the fourth most common cause of cancer-related death in the United States and carries a median survival of less than six months[1]. A small proportion of cases can be treated with potentially curative surgical resection, whereas most are locally advanced or metastatic at diagnosis[2]. The standard of care for advanced disease is chemotherapy which can range from single agent gemcitabine, with a modest extension in survival and relatively few side effects, to more effective combinations such as gemcitabine and abraxane or 5-fluorouracil, leucovorin, irinotecan, and oxaliplatin (FOLFIRINOX), though coming with a cost of increased toxicity[3]. A series of molecularly targeted therapies have failed to show benefit in clinical trials, and notably, unlike a number of other types of solid tumor types, genetically defined subsets of PDAC have yet to show acute response to specific inhibitors[2]. While the EGFR inhibitor erlotinib has been approved for PDAC in combination with gemcitabine, the survival benefit compared to gemcitabine alone is less than one month[4].

A number of factors likely conspire to produce poor therapeutic response of PDAC, including frequent diagnosis at advanced disease stage, high levels of genome instability with genetic variability across tumors in the same patient, and dense

fibroblastic stroma and poor perfusion that may limit drug delivery[2, 5]. An additional key element for the lack of response may be the high rate of activating KRAS mutations in these cancers (present in 70-95% of cases)[6]. Multiple lines of investigation point to a central role for activated KRAS in PDAC initiation as well as in tumor maintenance [7-11, 38]. Unfortunately, direct KRAS inhibitors have yet to be developed, and effective targeted therapy strategies for treating KRAS mutant cancers have remained elusive.

There is currently considerable interest in defining the critical KRAS effectors required for tumor maintenance since such factors may provide surrogate drug targets to extinguish the biological actions of KRAS. In this regard, the combined use of MEK and PI3K pathway inhibitors has been shown to be effective in KRAS-driven mouse models of lung cancer as well as in KRAS mutant colorectal cancer xenografts. Overall, the specific pathways activated by KRAS and the contributions of such pathways to tumor maintenance are likely to depend on tissue type and on the set of coincident genetic and epigenetic alterations. For instance, PI3K/Pdk1 signaling is selectively required for tumor initiation in Kras-driven PDAC, but not NSCLC, models[15]. In addition, recent studies have shown that, due to the existence of feedback control circuits in the pathway, inhibition of specific RAS signaling components can lead to unanticipated

augmentation of oncogenic signaling outputs[16]. Thus, as strategies to target various potential RAS effector pathways are being considered for future clinical trials, it is essential to apply relevant preclinical models as a guide to support a given therapeutic approach. More broadly, it will be important to define additional signaling dependencies in PDAC tumorigenesis.

Here, we sought to examine systematically the effect of a panel of known anti-cancer drugs on PDAC, and to then provide *in vivo* support for their therapeutic potential. To this end, we employed a large-scale screen of a set of well-characterized chemical inhibitors for their efficacy against a panel of more than 500 cell lines derived from a series of solid tumor types. Among the 50 compounds analyzed, this screen identified the MEK1/2 inhibitor, AZD-6244 (ARRY-142886)[19-20], as the most effective drug against PDAC cell lines. The capacity of AZD-6244 to promote apoptosis was significantly enhanced when combined with class I PI3K inhibitors. Moreover, this drug combination showed efficacy in a PDAC GEMM driven by mutations that define human PDAC, both delaying tumor onset when administered prior to tumor formation, and extending survival when used to treat established cancers. However, the effects were transient in both settings. While the promising results seen upon MEK and PI3K inhibition in other preclinical models have prompted

clinical trials of this regimen in KRAS mutant tumors, our results indicate that only limited benefit may be provided in the context of PDAC.

MATERIALS AND METHODS

Cell Lines

PDAC cell lines were grown in DMEM/F12 (GIBCO) with 10% FBS and assayed in DMEM/F12 with 5% FBS and were obtained from the MGH Center for Molecular Therapeutics (CMT), which performs routine cell line authentication testing by SNP and STR analysis.

High-throughput cell viability assay

Compounds were obtained from commercial sources or provided by AstraZeneca (Supplementary Table 1). Small molecule inhibitors were used at 3 concentrations 10 fold apart (see Supplementary Table 2). Cell viability was determined as previously described[28]. Briefly, cells were seeded in medium containing 5% FBS at density insuring cell growth throughout drug treatment (~15% for most cell lines). Drug treatment was started 24h post seeding and continued for 72 hours.

Cell were fixed and stained using Syto60 (Invitrogen) a red fluorescent DNA stain. Relative cell number was calculated by taking the ratio of the relative fluorescence intensity from drug treated wells over untreated wells after background subtraction (no cells seeded). Values are average from triplicate wells.

Annexin V Apoptosis Assays

Cells were seeded at ~30 to 40% confluence in 6 cm plates. After overnight incubation, media was aspirated and replaced with media with or without various concentrations of indicated drugs. After 72 hrs, media was collected. Cells were washed with PBS and trypsinized. PBS washed and trypsinized cells were added to the collected media in a single tube. Cells were pelleted, washed once with PBS and resuspended in Annexin binding buffer (BD Biosciences) at ~1 x 10^6 cells/mL. Cells were stained with propidium iodide (BD Biosciences) and Annexin V Cy5 (Biovision) according to the manufacturer's protocol and assayed on a LSRII flow cytometer (BD Biosciences).

Statistical Analysis

Relative efficacy of the compounds tested against PDAC cell lines was evaluated by comparing the viability of PDAC lines and non-PDAC lines for each compound. A Fisher exact test was used to determine statistical significance. For each compound the three concentrations tested were evaluated separately. The statistical test was iteratively run using a threshold of sensitivity corresponding to a cell viability of 10 to 80% by increment of 10% (the first test was done by classifying cell lines with viability of 10% or under as sensitive and cell lines with viability >10% as resistant). The minimum P value (one-tailed) obtained for a given compound across all concentrations and viability thresholds (24 tests per compound) was used to compare relative sensitivity of all compounds towards PDAC lines. All results of the Fisher exact test (two-tailed values) are in Supplementary table 2. Combination index to measure combined activity was analyzed with Compusyn (ComboSyn Inc.). To test tissue specific activity of AZD6244 a Fisher exact test was used to determine the statistical significance of the activity of AZD6244 at 2 uM against cell lines of different origin. For each tissue of origin viability of the cell lines was compared to viability of all lines from other tissue of origin. A threshold of 60% viability was used, other viability thresholds tested led to similar results. For each Tissue we compute the effect: Effect = Ln (Mean viability of All Other Lines / Mean viability of Tissue Lines). For the survival studies, statistical analysis was performed using

Prism statistical software version 4.0a May 11, 2003. Survival was determined using the Kaplan-Meir method and comparisons between treatment groups were determined using the Logrank test. Animals that displayed signs of illness and were found to have advanced cancers on necropsy were included as events. Animals that died for reasons other than advanced cancer were censored.

Mouse Strains and Histologic Analysis

The *Pdx1-Cre;LSL-KRAS^{G12D};p53$^{Lox/+}$* mouse PDAC model has been previously described[25]. Mice were housed in the pathogen-free environment maintained by the Center for Comparative Medicine (CCM) at the Massachusetts General Hospital. Mice were handled in strict accordance with good animal practice, as defined by the Subcommittee on Research Animal Care (SRAC) at Massachusetts General Hospital, and all mouse work was done with SRAC approval.

Chemical inhibitors

We purchased the MEK inhibitor ARRY-142886 (AZD6244) and GDC-0941 from commercial sources (Otava Chemicals). The PI3K inhibitor,

BKM-120, and the dual PI3K-mTOR inhibitor, NVP-BEZ235-AN, were obtained from Novartis Institutes for Biomedical Research. We reconstituted BKM-120 and AZD-6244 in one volume of N-methyl-2-pyrrolidone (69118, Fluka) and then added nine volumes of PEG300 (81160, Fluka), and administered these drugs by oral gavage daily at 50 mg/kg and 25 mg/kg, respectively. GDC-0941 was dissolved in 0.5% methylcellulose with 0.2% Tween-80 and administered by oral gavage at 75mg/kg daily. NVP-BEZ235-AN was reconstituted in 0.5% methyl cellulose (Fluka) and 0.4% polysorbate (Tween 80; Fluka) and administered daily by oral gave at a dosage of 25 mg/kg.

Western Blot analysis

Western blotting was performed using standard methods. Cells were washed with cold PBS and lysed in the following lysis buffer: 20 mM Tris pH 7.4, 150 mM NaCl, 1% Nonidet P-40, 10% glycerol, 1 mM EDTA, 1 mM EGTA, 5 mM sodium pyrophosphate, 50 mM NaF, 10 nM b–glycerophosphate, 1 mM sodium vanadate, 0.5 mM DTT, 4 mg/mL leupeptin, 4 mg/mL pepstatin, 4 mg/mL aprotinin, 1 mM phenylmethylsulfonyl fluoride. Lysates were centrifuged at 16,000 x *g* for 5 min at 4°C. Pancreatic tissues (100-200mg) were minced using a homogenizer, but otherwise processed as above. Protein

concentrations were determined by BCA assay (Thermo Scientific). Proteins were resolved by SDS-PAGE and transferred to a polyvinylidene difluoride membrane (Hybond-P, Amersham). Immunoblotting was performed per antibody manufacturer's specifications.

Immunofluorescence and Immunohistochemistry

Samples were fixed in 10% formalin and embedded in paraffin. After deparaffinization, slides were washed with 9.83% NaCl for 3 min followed by a PBS wash and a wash in distilled water for 5 min. Heat induced antigen retrieval was performed with pressure cooker (2100 Retriever, PickCell Laboratories B.V.) and R-Buffer A (pH6.0, Electron Microscopy Sciences). Sections were incubated with 2% H_2O_2 in Methanol for 15 minutes for endogenous peroxidase quenching and washed and blocked for non-specific binding in 1% BSA in PBS-Triton 0.3% v/v (PBST) for 1 hour. Subsequently, sections were sequentially incubated with primary antibody at 1:100 dilution for 1 hour, secondary peroxidase goat anti-rabbit IgG antibody (Vector) at 1:250 dilution for 1 hour and Tyramide Signal Amplification (TSA) Fluorescein System (Perkin Elmer, Cat.: NEL701A) according to kit manual. Slides were mounted with Vectashield mounting medium

with DAPI (Vector), photographed with Nikon C2 Confocal Microscope system and subsequently stained with Hematoxylin and Eosin. p-AKT (Thr308) p-ERK (Thr202/Tyr204), p-S6 (Ser235/236), and CC3 (Asp 175) were analyzed at the indicated site (Cell Signaling, Inc). Ki67 staining was performed as previously described[31]. Quantification of Ki67 staining was performed by scoring the nuclei of cells from each lesion type found in a minimum of ten high-powered fields.

Organotypic Tissue Cultures.

Organotypic tissue cultures were prepared from primary PDAC using previously described methods[26]. In brief a Vibratome VT1200 (Leica Microsystems) was used to cut thin (300–500 mm) slices from fresh tissue. Tissue slices were cultured on organotypic inserts (Teflon membranes with 0.4-µm pores) for up to 120 h (two slices per insert; Millipore). Tissue culture was performed at 37 °C in a 5% CO2 humidified incubator using 1 ml of Ham F-12 media supplemented with 20% inactivated FBS (GIBCO), 100 U/mL penicillin (Invitrogen), 100 µg/mL streptomycin (GIBCO), 2.5 µg/mL amphoterycin B, and 100 µg/mL of kanamycin (Sigma Aldrich). Medium was changed every 2 days. Tissue slices were harvested at baseline time (T0) and

thereafter, at 24-h intervals; slices was formalin-fixed and paraffin-embedded for morphological (H&E) and IHC evaluation.

Magnetic Resonance

MRI measurements were performed using a 4.7 T Bruker Avance horizontal bore system equipped with a 200 mm inner diameter gradient set capable of 30G/cm gradient strength. The mice were anesthetized with 1% isoflurane in an oxygen/air mixture. The animals' respiratory and cardiac rates were monitored using Biotrig Software. The animals were imaged with T2 weighted turbo spin echo (RARE) sequence (TR = 2000 ms, TE effect = 36 ms, echo train length =4, number of averages =8) in the coronal planes with a 0.9mm slice thickness and with the number of slices sufficient to cover the entire abdomen, and with a matrix size of 256 x 256, field of view (FOV) of 4 x 5.5 cm2, resulting in an in-plane resolution of .25 x .12 mm. With the same geometry as described above, the animals were also imaged with a T1-weighted RARE sequence (TR=900ms, TE effective = 14msec.) and parameters equivalent to the T2 weighted sequence described above with respiratory and cardiac gating, in both the coronal and axial planes prior to and following the intravenous administration of 0.3 mmol/kg of Gd-DTPA (Magnevist;

Schering, Berlin, Germany). Using the post-contrast sequence scans, volume measurements of the tumors were performed using in-house customized software on an Osirix ® (Lausanne, Switzerland). In specific, the longest diameter in each plane (anterior posterior, right-left, and cranial-caudal) were measured and multiplied as a product of the perpendicular diameters (PPD).

RESULTS AND DISCUSSION

Screening of a panel of anti-cancer drugs identifies MEK inhibitors as compounds with highest efficacy in PDAC cell lines

In order to identify drugs that show selective efficacy in PDAC, we conducted a high-throughput cell line screen that examined the responsiveness of human cancer cell lines to a panel of 50 clinically relevant small molecule compounds (consisting mainly of rationally designed agents, Supplementary Table 1). The screen incorporated >500 human cancer cell lines, including 46 PDAC lines. Statistical analysis of the sensitivity of PDAC lines relative to all other lines shows that for the majority of compounds, PDAC cell lines were significantly less sensitive than non-PDAC cells (Figure 1A, red dots compared to green dots). Moreover, we did not observe subsets of

PDAC cell lines that showed acute sensitivity to any of the compounds (data not shown). Thus, the general therapeutic resistance of PDAC appears to be recapitulated in cultured cell lines.

In spite of the overall resistance of the PDAC cell lines, we did observe that a small number of compounds showed selective activity in this cancer type (Figure 1A, green dots). Erlotinib, the only approved targeted therapy for PDAC (approved in combination with gemcitabine[4]), was among the top hits, supporting that this approach can accurately identify compounds with clinical activity in PDAC. Among these compounds, the MEK kinase inhibitor, AZD-6244, clearly stood out as having the greatest relative efficacy in PDAC (see Figure 1A showing that AZD-6244 has highest effect and p value of the PDAC-selective compounds). Notably, >90% of the PDAC cell lines have activating KRAS mutations, and MEK inhibitors were found to be the most effective compounds against KRAS mutant cancers across all tumor types examined[21]. Previous studies have shown that KRAS mutant PDAC cell lines can be divided into subsets that have either a high or a low dependency on KRAS activity for proliferation as assessed by KRAS knockdown[11, 22]. The cell lines in either group showed overlapping sensitivity profiles to AZD-6244 (Figure 1B), consistent with MEK serving as an important mediator of PDAC growth across molecularly distinct subsets of PDAC.

Although AZD-6244 was the most effective compound in PDAC cell lines, the overall magnitude of the responses was weak as compared to that of melanoma lines, a majority of which harbor sensitizing BRAF mutations (Figure 1C and D). Thus, these *in vitro* studies support the further evaluation of MEK inhibitors in PDAC but suggest that their activity as a single-agent therapies may be limited.

Combinatorial effects of dual MEK and PI3K inhibition on apoptosis in PDAC cell lines

For many drugs, the capacity to induce apoptosis *in vitro* is a better predictor of *in vivo* efficacy than cell cycle arrest[20, 21]. Since our high-throughput assay does not distinguish between growth arrest and induction of cell death, we examined directly the impact of AZD-6244 on apoptosis in a panel of PDAC cell lines. This compound induced modest levels of apoptosis relative to vehicle in most cell lines, despite effectively downregulating phospho-ERK levels (Figure 2A, B, and Supplementary Figure 1A). Since prior studies have shown that inhibitors of the PI3K survival pathway can enhance the efficacy of MEK inhibition in other KRAS mutant cancers[13], we also studied the apoptotic potential of the PI3K inhibitors, BKM-120 and GDC-0941. Both compounds caused small increases in apoptosis as single

agents in PDAC cell lines but, when combined with MEK inhibitors, acted either additively or synergistically to significantly augment levels of apoptosis in most PDAC lines (Figure 2A, B, and Supplementary Figure 1A), supporting the combined use of these compounds.

Efficacy of dual MEK and PI3K inhibition in ex vivo organotypic models derived from primary PDAC

We next sought to test the impact of single or dual MEK/PI3K inhibition in primary tumors. Consistent with previous studies[25-28], IHC analysis of human PDAC showed staining for both phospho-ERK and phospho-AKT in the tumor epithelium, indicating ongoing activation of these pathways (Supplementary Figure 1B). We first tested the efficacy of AZD-6244 and BKM-120 in an *ex vivo* organotypic model[29, 26]. This model, which employs thin (300–500 mm) sections of primary tumors obtained using a vibratome (see Materials and Methods), enables evaluation of therapeutic efficacy in the context of preserved tumor-stroma interactions and 3-D architecture. Treatment of sections of the same tumor with AZD-6244 or BKM-120 extinguished p-ERK staining and p-AKT staining, respectively, and the combination caused loss of both signals (Figure

2C). Although these compounds induced apoptosis (cleaved-caspase-3 staining) and reduced proliferation (Ki-67 staining) when used as single-agent, their combination resulted in significantly more pronounced effects (Figure 2C; data are quantified in Figure 2D and E). These alterations were most notable in the tumor epithelium rather than the stroma.

Dual MEK/PI3K inhibition delays PDAC initiation and progression in the KRAS-p53 mouse model

We next sought to establish the impact of MEK/PI3K inhibition on primary PDAC *in vivo*. We used a genetically engineered mouse model (GEMM) of PDAC driven by activation of KRAS and inactivation of p53 (*Pdx1-Cre; LSL-KRAS^{G12D}; p53$^{Lox/+}$*, designated KRAS-p53 mice) that recapitulates the genetics and histopathologic progression of the human disease in a synchronous and predictable manner[27]. First, we investigated the potential of AZD-6244 and BKM-120 to limit the initiation and progression of PDAC when administered prior to the onset of frank tumors. As shown in the study design schematic in Figure 3A, mice were treated with these compounds starting at 8 weeks of age, a time point when only pre-invasive pancreatic ductal lesions (pancreatic intraepithelial

neoplasias; PanINs) are present[27]. The impact of these drugs was compared with vehicle control and with gemcitabine, which is the current standard of care for PDAC. The drugs were well-tolerated as single agents and in combination, consistent with reports using other MEK and PI3K inhibitors[13]. In this setting, the combination of AZD-6244 and BKM-120 gave the strongest protective effect, nearly doubling the length of survival compared to controls (median 131.5 days versus 71 days)(Figure 3B and C). Single agent treatment with AZD-6244, BKM-120, or gemcitabine produced an intermediate extension in survival (Figure 3B and C). As shown in Supplementary Figure 2, we also observed a significant extension of survival in a prevention study using AZD-6244 combined with the dual specificity PI3K/mTOR inhibitor, BEZ-235 (85.2 days compared to 44.5 days for controls, $p<0.001$)—in these studies, treatment was initiated at 10 weeks when disease is slightly more advanced, consisting of higher grade PanINs or early PDAC. Despite the extension in lifespan conferred by the inhibitors, all mice eventually developed pancreatic tumors. Histological examination showed that the tumors arising in all groups had comparable pathological histological features, consisting of invasive, well-differentiated to poorly-differentiated PDAC (data not shown). Thus, dual MEK/PI3K inhibition significantly delays the initiation and malignant progression of PDAC while not

strongly altering the intrinsic malignant phenotype of the tumors that eventually arise.

Dual MEK/PI3K inhibition induces response in advanced PDAC

We conducted therapeutic studies in the more clinically relevant setting of advanced PDAC. Mice were examined for the presence of established tumors using MRI beginning at the age of 12 weeks and then randomized into treatment groups (control, AZD-6244, PI3K inhibitor (either BKM-120 or GDC-0941)). Serial MRI was used to monitor changes in tumor volume (the study design is shown in Figure 4A). Whereas progressive disease was observed in all mice treated with vehicle, or the single MEK and PI3K inhibitors, combined MEK/PI3K inhibition for 7 days resulted in initial reduction in tumor size in 8/10 mice (Figure 4B; representative three-dimensional renderings of MRI scans are shown in Figure 4C). Immunohistochemical analysis showed that p-AKT, p-ERK , and p-S6 levels in the tumors were effectively reduced upon administration of AZD-6244 and BKM-120, respectively, as compared to vehicle treated controls, indicating robust targeting of the MEK and PI3K pathways (Figure 4D and Supplementary Figure 3A). Of note, suppression of TORC1 signaling, as evidenced by p-S6, required concomitant

inhibition of both PI3K and MEK, consistent with our earlier findings in a lung cancer GEMM[13] (Figure 4D).

The responses seen by MRI in the mice treated with the dual inhibitor regimen translated into a temporally sustained control of the disease burden increase in survival after diagnosis. Whereas the control group had a median survival of 27 days after tumor detection, mice treated with the combination lived a median of 59 days (Figure 5A). By comparison, AZD-6244 provided no survival benefit, and BKM-120 had an intermediate effect. Serial MRI showed that the effects of the combination were transient, with most tumors showing increasing size within 2-3 weeks of treatment (representative data shown in Figure 5B). On histology, we found that tumors, in which MRI response was identified, show marked surrounding fibrosis and reduced parenchymal invasion when compared to controls (Supplementary Figure 3B). Thus, combined targeting of MEK and PI3K provides clinically significant responses in a genetically and histologically faithful GEMM of PDAC, although the regimen is not curative and does not produce a durable response. Together with the findings presented by Junttila et al. (submitted), the present data suggest that while the combination may not offer marked improvement over the current standard of care for PDAC, but it may be beneficial as an alternative or second-line treatment. Although we

cannot rule out that the moderate responses were due to limited drug delivery to the tumors, our short term signaling studies indicated that the target pathways were effectively suppressed. Additionally, our studies in the prevention setting, where there is initially limited stroma, revealed only a limited delay in tumor development. These findings are in contrast with KRAS-driven murine lung cancers which show pronounced and sustained responses to dual MEK/PI3K inhibition. Notably, genetic studies in mouse models of KRAS mutant lung cancer, colon cancer, and PDAC show that there are multiple differences in their requirements for pathways downstream or intersecting with KRAS for tumorigenicity, suggesting that alternatives therapeutic strategies will be required[15,37].

The biggest advances in treatment have come from retooled versions of long-standing cancer drugs — abraxane and gemcitabine or combinations of drugs commonly used in other diseases[3]. These new effective chemotherapy choices have had a significant positive impact on patients but further incremental improvements using similar approaches are likely to be limited by the increasing toxicity and side effects of multi-layered cytotoxic chemotherapy. One of the biggest question clinical investigators face is how to choose drugs to test clinically from among the many new agents available and gaining traction in other cancers. In light of the increasingly limited federal

resources this is a significant problem and being able to demonstrate in preclinical models agents with limited effectiveness may help to direct these resources more effectively. Just how studies, using these preclinical GEM models, should be used to guide clinical development remains an open question, and the ongoing evaluation of preclinical models in light of clinical trial results will be important to understand how to best use these models.

ACKNOWLEDGEMENTS

This work was supported by grants to N.B. from the AACR/Pancreatic Cancer Action Network, the NIH (NCI 2P01CA117969-06), and Dana-Farber/Harvard Cancer Center Gastrointestinal Cancer SPORE grant P50 CA127003 (to N.B. and J.A.E.). R.B.C was supported by NIH training grant T32 CA071345. G.C. was supported by Fondazione Umberto Veronesi, Associazione Italiana per la ricerca sul Cancro, and American Italian Cancer Foundation.

REFERENCES

1. Jemal A, Siegel R, Xu J, Ward E. Cancer statistics, 2010. CA Cancer J Clin 2010;60:277-300.
2. Hidalgo M. Pancreatic cancer. N Engl J Med 2010;362:1605-17.
3. Conroy T, Desseigne F, Ychou M, Bouche' O, Guimabud R, Bécouarn Y, et al. FOLFIRINOX versus gemcitabine for metastatic pancreatic cancer. N Engl J Med 2011;364:1817-25.
4. Moore MJ, Goldstein D, Hamm J, Figer A, Hecht JR, Gallinger S, et al. Erlotinib plus gemcitabine compared with gemcitabine alone in patients with advanced pancreatic cancer: a phase III trial of the National Cancer Institute of Canada Clinical Trials Group. J Clin Oncol 2007;25:1960-6.
5. Olive KP, Jacobetz MA, Davidson CJ, Gopinathan A, McIntyre D, Honess D, et al. Inhibition of Hedgehog signaling enhances delivery of chemotherapy in a mouse model of pancreatic cancer. Science 2009;324:1457-61.
6. Jones S, Zhang X, Parsons DW, Lin JC, Leary RJ, Angenendt P, et al. Core signaling pathways in human pancreatic cancers revealed by global genomic analyses. Science 2008;321:1801-6.
7. Moskaluk CA, Hruban RH, Kern SE. p16 and K-ras gene mutations in the intraductal precursors of human pancreatic adenocarcinoma. Cancer Res 1997;57:2140-3.

8. Hruban RH, Wilentz RE, Kern SE. Genetic progression in the pancreatic ducts. Am J Pathol 2000;156:1821-5.
9. Hingorani SR, Petricoin EF, Maitra A, Rajapakse V, King C, Jacobetz MA, et al. Preinvasive and invasive ductal pancreatic cancer and its early detection in the mouse. Cancer Cell 2003;4:437-50.
10. Aguirre AJ, Bardeesy N, Sinha M, Lopez L, Tuveson DA, Horner J, et al. Activated Kras and Ink4a/Arf deficiency cooperate to produce metastatic pancreatic ductal adenocarcinoma. Genes Dev 2003;17:3112-26.
11. Singh A, Greninger P, Rhodes D, Koopman L, Violette S, Bardeesy N, et al. A gene expression signature associated with "K-Ras addiction" reveals regulators of EMT and tumor cell survival. Cancer Cell 2009;15:489-500.
12. Halilovic E, She QB, Ye Q, Pagliarini R, Sellers WR, Solit DB, et al. PIK3CA mutation uncouples tumor growth and cyclin D1 regulation from MEK/ERK and mutant KRAS signaling. Cancer Res 2010;70:6804-14.
13. Engelman JA, Chen L, Tan X, Crosby K, Guimaraes AR, Upadhyay R, et al. Effective use of PI3K and MEK inhibitors to treat mutant Kras G12D and PIK3CA H1047R murine lung cancers. Nat Med 2008;14:1351-6.

14. Roberts PJ, Usary JE, Darr DB, Dillon PM, Pfefferle AD, Whittle MC, et al. Combined PI3K/mTOR and MEK inhibition provides broad antitumor activity in faithful murine cancer models. Clin Cancer Res. 2012 Oct 1;18(19):5290-303.
15. Eser S, Reiff N, Messer M, Seidler B, Gottschalk K, Dobler M, et al. Selective Requirement of PI3K/PDK1 Signaling for Kras Oncogene-Driven Pancreatic Cell Plasticity and Cancer. Cancer Cell. 2013 Mar 18;23(3):406-20.
16. Lim KH, Baines AT, Fiordalisi JJ, Shipitsin M, Feig LA, Cox AD, et al. Activation of RalA is critical for Ras-induced tumorigenesis of human cells. Cancer Cell 2005;7:533-45.
17. Lim KH, Counter CM. Reduction in the requirement of oncogenic Ras signaling to activation of PI3K/AKT pathway during tumor maintenance. Cancer Cell 2005;8:381-92.
18. Cox AD, Der CJ. The raf inhibitor paradox: unexpected consequences of targeted drugs. Cancer Cell 2010;17:221-3.
19. Yeh TC, Marsh V, Bernat BA, Ballard J, Colwell H, Evans RJ, et al. Biological characterization of ARRY-142886 (AZD6244), a potent, highly selective mitogen-activated protein kinase kinase 1/2 inhibitor. Clin Cancer Res 2007;13:1576-83.
20. Adjei AA, Cohen RB, Franklin W, Morris C, Wilson D, Molina JR, et al. Phase I pharmacokinetic and pharmacodynamic study of the oral, small-molecule mitogen-activated protein kinase

kinase 1/2 inhibitor AZD6244 (ARRY-142886) in patients with advanced cancers. J Clin Oncol 2008;26:2139-46.

21. Garnett MJ, Edelman EJ, Heidorn SJ, Greenman CD, Dastur A, Lau KW, et al. Systematic identification of genomic markers of drug sensitivity in cancer cells. Nature. 2012 Mar 28;483(7391):570-5.
22. Collisson EA, Sadanandam A, Olson P, Gibb WJ, Truitt M, Gu S, et al. Subtypes of pancreatic ductal adenocarcinoma and their differing responses to therapy. Nat Med 2011;17:500-3.
23. Faber AC, Li D, Song Y, Liang MC, Yeap BY, Bronson RT, et al. Differential induction of apoptosis in HER2 and EGFR addicted cancers following PI3K inhibition. Proc Natl Acad Sci U S A 2009;106:19503-8.
24. Faber AC, Corcoran RB, Ebi H, Sequist LV, Waltman BA, Chung E, et al. BIM Expression in Treatment-Naïve Cancers Predicts Responsiveness to Kinase Inhibitors. Cancer Discovery 2011.
25. Yamamoto S, Tomita Y, Hoshida Y, Morooka T, Nagano H, Dono K, et al. Prognostic significance of activated Akt expression in pancreatic ductal adenocarcinoma. Clin Cancer Res 2004;10:2846-50.
26. Kennedy AL, Morton JP, Manoharan I, Nelson DM, Jamieson NB, Pawlikowski JS, et al. Activation of the PIK3CA/AKT

pathway suppresses senescence induced by an activated RAS oncogene to promote tumorigenesis. Mol Cell 2011;42:36-49.

27. Hill R, Calvopina JH, Kim C, Wang Y, Dawson DW, Donahue TR, et al. PTEN loss accelerates KrasG12D-induced pancreatic cancer development. Cancer Res 2010;70:7114-24.
28. Vaira V, Fedele G, Pyne S, et al. Preclinical model of organotypic culture for pharmacodynamic profiling of human tumors. Proc Natl Acad Sci U S A 2010;107:8352-6.
29. Bardeesy N, Aguirre AJ, Chu GC, Cheng KH, Lopez LV, Hezel AF, et al. Both p16(Ink4a) and the p19(Arf)-p53 pathway constrain progression of pancreatic adenocarcinoma in the mouse. Proc Natl Acad Sci U S A 2006;103:5947-52.
30. Infante JR, Fecher LA, Falchook GS, Nallapareddy S, Gordon MS, Becerra C, et al. Safety, pharmacokinetic, pharmacodynamic, and efficacy data for the oral MEK inhibitor trametinib: a phase 1 dose-escalation trial. Lancet Oncol. 2012 Aug;13(8):773-81. doi: 10.1016/S1470-2045(12)70270-X.
31. Falchook GS, Lewis KD, Infante JR, Gordon MS, Vogelzang NJ, DeMarini DJ, et al. Activity of the oral MEK inhibitor trametinib in patients with advanced melanoma: a phase 1 dose-escalation trial. Lancet Oncol. 2012 Aug;13(8):782-9. doi: 10.1016/S1470-2045(12)70269-3.

32. Singh M, Lima A, Molina R, Hamilton P, Clermont AC, Devasthali V, et al. Assessing therapeutic responses in Kras mutant cancers using genetically engineered mouse models. Nat Biotechnol 2010;28:585-93.
33. Feldmann G, Habbe N, Dhara S, Bisht S, Alvarez H, Fendrich V, et al. Hedgehog inhibition prolongs survival in a genetically engineered mouse model of pancreatic cancer. Gut 2008;57:1420-30.
34. Morton JP, Karim SA, Graham K, Timpson P, Jamieson N, Athineos D, et al. Dasatinib inhibits the development of metastases in a mouse model of pancreatic ductal adenocarcinoma. Gastroenterology 2010;139:292-303.
35. Brachmann SM, Kleylein-Sohn J, Gaulis S, Kauffmann A, Blommers MJ, Kazic-Legueux M, et al. Characterization of the mechanism of action of the pan class I PI3K inhibitor NVP-BKM120 across a broad range of concentrations. Mol Cancer Ther. 2012 Aug;11(8):1747-57.
36. Zhou D, Conrad C, Xia F, Park JS, Payer B, Yin Y, et al. Mst1 and Mst2 maintain hepatocyte quiescence and suppress hepatocellular carcinoma development through inactivation of the Yap1 oncogene. Cancer Cell 2009;16:425-38.
37. Navas C, Hernández-Porras I, Schuhmacher AJ, Sibilia M, Guerra C, Barbacid M. EGF receptor signaling is essential for k-

ras oncogene-driven pancreatic ductal adenocarcinoma. Cancer Cell. 2012 Sep 11;22(3):318-30.

38. Ying H, Kimmelman AC, Lyssiotis CA, Hua S, Chu GC, Fletcher-Sananikone E, et al. Oncogenic Kras maintains pancreatic tumors through regulation of anabolic glucose metabolism. Cell. 2012 Apr 27;149(3):656-70.

FIGURES

Figure 1

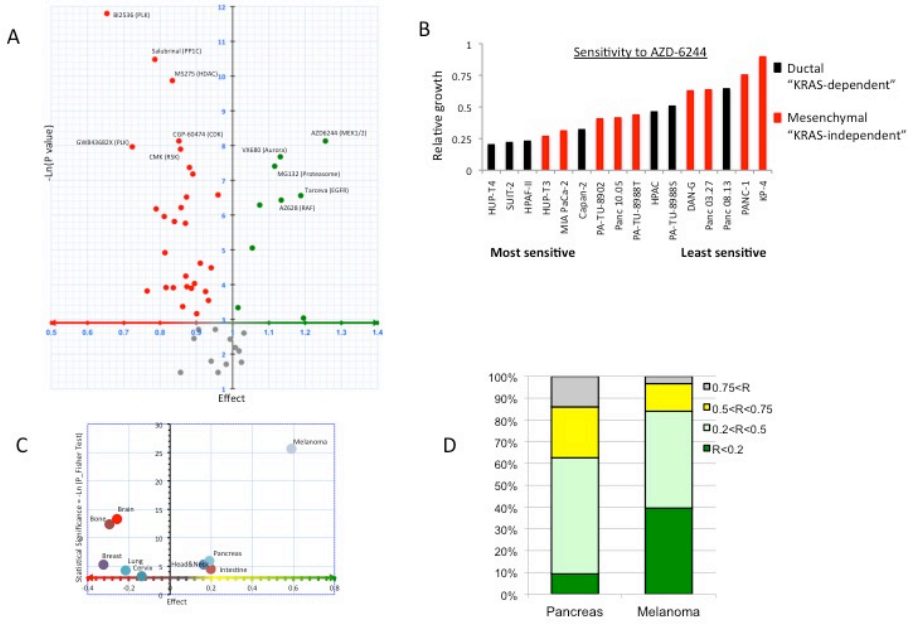

Figure 1. **High-throughput screening identifies the MEK1/2 inhibitor, AZD6244 as the most active compound against PDAC cell lines.**

A) Volcano plot representing the responsiveness of PDAC cell lines (N=46) compared to non-PDAC cancer cell lines (N=500) to a series of 50 potential anti-cancer drugs. X axis: relative sensitivity (Effect > 1: PDAC cells are on average more sensitive than non-PDAC cells), Y axis: statistical significance (Gray dots: compounds with p>0.05; Green dots: compounds preferentially targeting PDAC; Red dots: compounds for which PDAC cell lines are more resistant than other types of cell lines).

B) Relative sensitivity to AZD-6244 of PDAC cell lines identified as "KRAS-dependent" and "–independent"[11, 19]. ***C)*** Organ specificity profile of AZD-6244. Cell lines from cancer types were iteratively compared to the rest of the cell collection to determine the specific targeting by tissue of origin. X axis: relative sensitivity (Effect: average survival of cell lines from a given organ/survival of the other lines). Y axis: statistical significance of the organ enrichment (Fisher exact test). ***D)*** Relative sensitivity of PDAC and melanoma lines to 2 mM AZD-6244. Bar color indicates relative cell number (R) compared to control. Bar height represents the percentage of cell lines of each tumor type showing the indicated degree of growth inhibition.

Figure 2

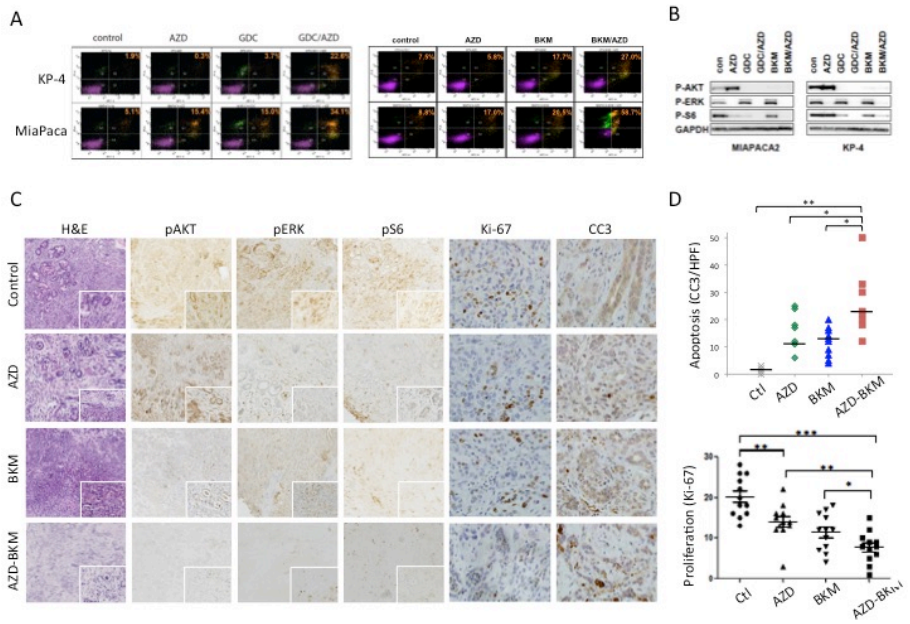

Figure 2. Analysis of cell lines and ex vivo organotypic cultures supports the combined targeting of MEK and PI3K in PDAC.

A, B) Treatment of PDAC cell lines with vehicle control or with the indicated drugs (AZD: AZD-6244; BKM: BKM-120; GDC: GDC-0941) used at 1 mM. ***A)*** FACS plots showing PI/AnnexinV staining. The % of apoptotic cells is indicated. ***B)*** Western blot showing effect of the inhibitors on p-AKT (Thr308) and p-ERK (Thr202/Tyr204) levels.

C-D) Analysis of therapeutic responses of *ex vivo* organotypic cultures of primary PDAC. ***C)*** Freshly derived organotypic cultures were treated with the indicated compounds (each at 1 mM) for 24 hours and then processed for staining with H&E or with antibodies to p-ERK (Thr202/Tyr204), p-AKT (Thr308), p-S6 (Ser235/236), Ki-67, and cleaved Caspase 3. ***D)*** Quantification of apoptosis at 24 hrs (cleaved caspase-3 staining) and of proliferation (Ki-67 staining). Statistical significance is indicated; $p<0.01$ (*), $p<0.0001$ (**).

Figure 3

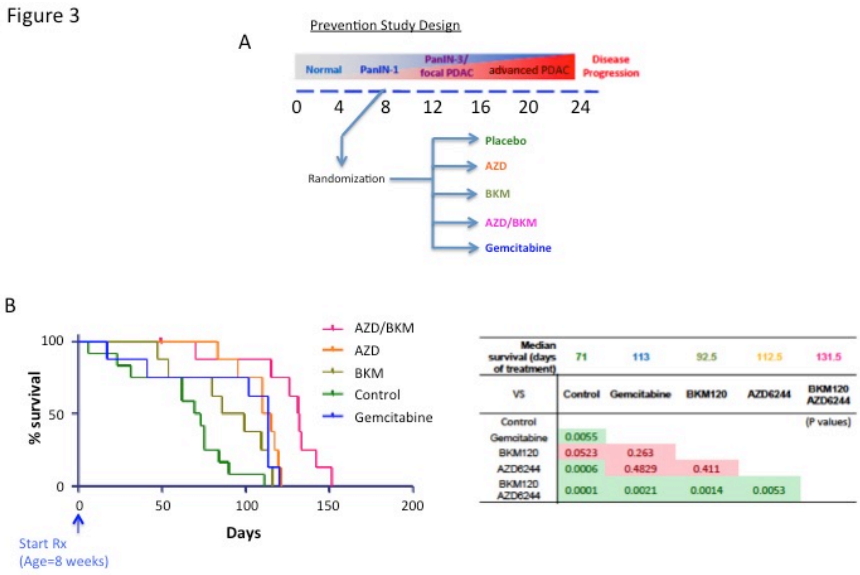

Median survival (days of treatment)	71	113	92.5	112.5	131.5
VS	Control	Gemcitabine	BKM120	AZD6244	BKM120 AZD6244
Control					(P values)
Gemcitabine	0.0055				
BKM120	0.0523	0.263			
AZD6244	0.0006	0.4829	0.411		
BKM120 AZD6244	0.0001	0.0021	0.0014	0.0053	

Figure 3. Combined targeting of MEK and PI3K delays the progression of PDAC from PanIN lesions in the KRAS-p53 mouse model.

A) Schematic of experimental design for prevention studies. Mice were treated prior to the onset of PDAC and monitored for evidence of tumor progression.

B) Survival curve (Kaplan-Meier Analysis) calculated as length of time between start of treatment and sacrifice.

C) Chart showing statistical analysis of survival data.

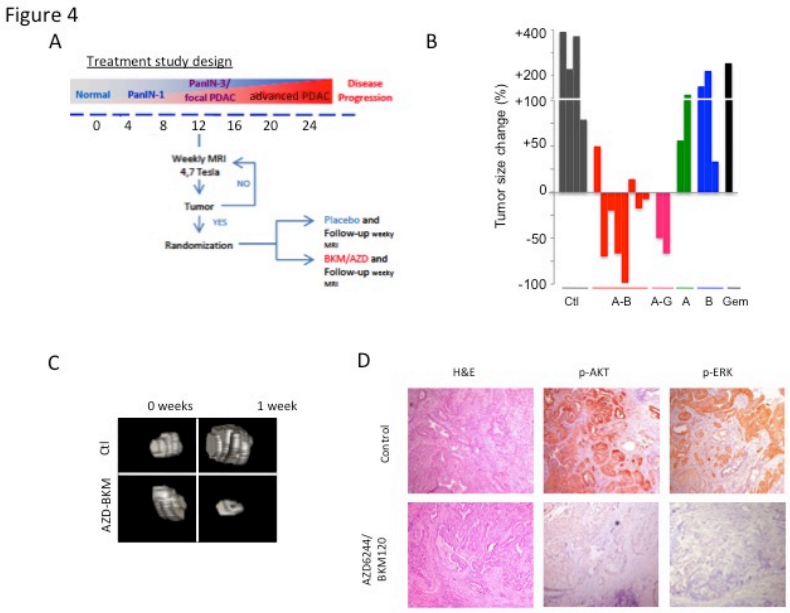

Figure 4. Advanced PDAC in the KRAS-p53 mouse model are responsive to dual MEK/PI3K inhibition.

A) Schematic of experimental design for treatment of advanced PDAC. Mice were monitored for the presence of tumors by MRI. Upon detection of PDAC 3-10 mm in size, mice were randomized into the treatment and control groups.

B) Waterfall plot showing efficacy of AZD-6244 (A) combined with either BKM-120 (B) or GDC-0941 (G) in promoting PDAC regression. No responses were seen with the single agents or with gemcitabine (Gem). Statistical significance: combination versus control ($p<0.0001$), versus AZD-6244 ($p<0.01$), versus BKM-120 ($p<0.001$).

C) Representative three-dimensional reconstructions of MRI scans prior to treatment, or after 1 week in the indicated treatment groups.

D) Immunohistochemical staining for p-ERK (Thr202/Tyr204) and p-S6 (Ser235/236), in PDAC isolated from KRAS-p53 mice treated for 1 week with the indicated compounds.

Figure 5

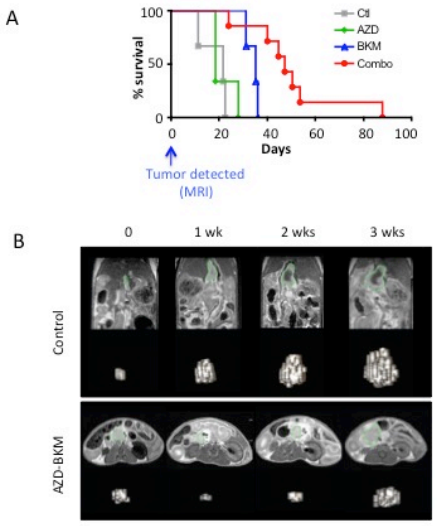

Figure 5. Clinical benefit of dual MEK/PI3K inhibition in the KRAS-p53 and KRAS-PTEN mouse PDAC models

A) Survival curve (Kaplan-Meier analysis) of KRAS-53 mice after MRI detection of PDAC and administration of the indicated treatments. The differences between the AZD-6244/BKM-120 combination and the other groups are statically significant (compared to control, p=0.0008; compared to AZD, p=0.0061; compared to BKM, p=0.022).

B) Representative MRI scans of KRAS-p53 mice and 3D reconstructions at sequential time points in the indicated treatment groups. The vehicle-treated mouse show rapid tumor progression (upper panel). Treatment with AZD-6244 and BKM-120 results in partial tumor regression in some mice, although the effects are transient.

SUPPLEMENTARY FIGURE LEGENDS

Supplementary Figure 1. MEK and PI3K pathways in human PDA.

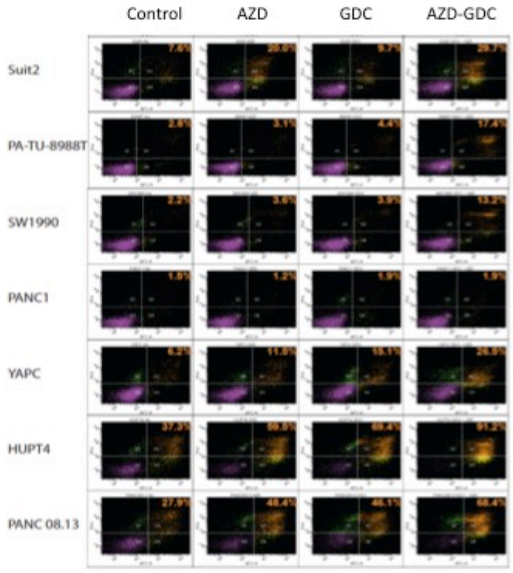

A. FACS plots showing PI/AnnexinV staining of human PDAC cell lines treated with vehicle control or with the indicated drugs (AZD: AZD-6244; GDC: GDC-0941).

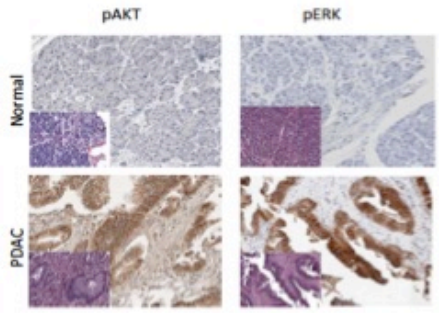

B. Immunohistochemical analysis of p-ERK (Thr202/Tyr204) and p-AKT (Thr308) staining in human PDAC and in normal human pancreas.

Supplementary Figure 2. Combination treatment with the MEK1/2 inhibitor, AZD-6244, and the dual PI3K/mTOR inhibitor, BEZ-235, extends survival in the KRAS-p53 mouse PDAC model

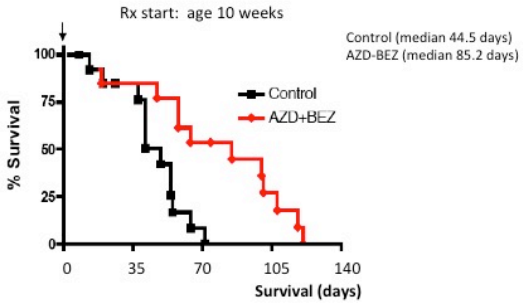

Kaplan-Meier curve showing tumor-free survival of control and AZD-6244/BEZ-235 treated mice. Treatment was started at an age of 10 weeks of age, a time point where advanced PanINs or focal PDAC are present. Mice were euthanized upon the appearance of clinical signs of illness.

c 3. Response of advanced PDAC GEM model to MEK and PI3K inhibition.

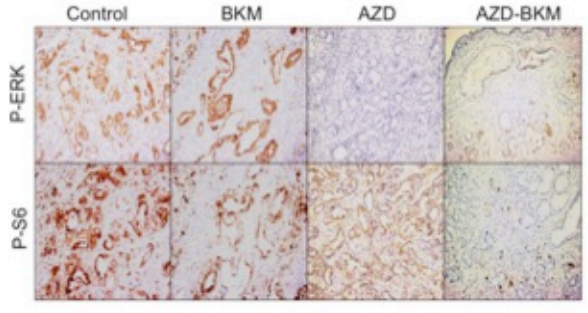

A. Immunohistochemical staining for p-ERK (Thr202/Tyr204) and p-AKT (Thr308), in PDAC isolated from KRAS-p53 mice treated for 7 days with the indicated compounds.

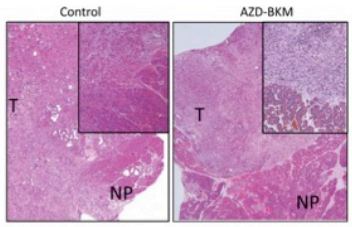

T, Tumor; NP, Normal Parenchyma

B. H&E stained sections of (*Left panel*) untreated PDAC, and (*Right panel*) PDAC treated with the combination of AZD-6244 and BKM-120 for 9 days. The tumor (T) shows invasion into the normal pancreatic tissue (NP) in the control mouse whereas the treated mouse shows well-circumscribed tumor boundaries.

Supplementary table 1

Compound_Name	Target_HUGO	Source	PUBchem	Molecular Weight	[Max] uM	Effect (PDAC/Non PDAC)	P_Value (one-tailed)
BI-2536	PLK1, PLK2,PLK3	haoyuan chemexpress	11364421	521.31	0.5	0.653081436	0.000007471
Salubrinal	PPP1R15A	Tocris	5717801	479.8	15	0.785341969	0.000027991
MS-275	HDAC	LC Labs	4261	376.41	10	0.834038352	0.000051651
CGP-60474	CDK1,CDK2,CDK5,CDk7,CDK9	haoyuan chemexpress	644215	355.12	0.5	0.851960825	0.000293813
AZD6244	MAP2K1, MAP2K2	AstraZeneca	10127622	457.68	20	1.255667835	0.000294001
GSK461364	PLK1	haoyuan chemexpress	15983966	543.2	0.5	0.723058401	0.000346905
cmk	RPS6KA1	Nathanael Gray	NA	344.1	2	0.856439193	0.000372187
VX680	AURKA	haoyuan chemexpress	5494449	464.21	2	1.131728703	0.000463296
MG-132	PSMB	haoyuan chemexpress	462382	475.6	1	1.116210046	0.000606140
Rapamycin	MTOR	LKT Laboratories	5284616	914.17	10	0.880894634	0.000629623
JW-5-8-1	PIK3CA, MTOR	Nathanael Gray	NA	530.54	0.5	0.890250728	0.000760252
BMS-509744	ITK	haoyuan chemexpress	20635522	609.24	2	0.959892107	0.001386262
Erlotinib	EGFR	MGH Pharmacy	176870	393.44	2	1.188148204	0.001415548
Z-LLNle-CHO / Z-LL-Norleucine-CHO	PSEN1	EMD Biosciences	16760646	475.62	5	0.873062163	0.001477745
AZ628	BRAF	haoyuan chemexpress	11676786	451.53	2	1.133928754	0.001609727
Cyclopamine	SMO	haoyuan chemexpress	442972	411.62	10	1.074714811	0.001856289
Lapatinib	EGFR, ERBB2	haoyuan chemexpress	208908	925.5	2	0.858032688	0.002000602
S-Trityl-L-cysteine	KIF11	haoyuan chemexpress	76044	363.47	5	0.789060368	0.002069713
GO-6976	PKC	haoyuan chemexpress	3501	378.4259	10	0.811573771	0.002582620
Sunitinib	KDR,c-Kit, PDGFR, FLT3	MGH Pharmacy	5329102	398.5	10	0.839465605	0.002985540
A-443654	AKT1,AKT2,AKT3	haoyuan chemexpress	10172943	397.2	2.5	0.869953739	0.003144728
TAE684	ALK	haoyuan chemexpress	16038120	613.26	2	1.054245689	0.006388123
KN-93	CAMK2	haoyuan chemexpress	5312122	501.04	10	0.813480966	0.007326302
LY294002	MTOR, PIK3CA	haoyuan chemexpress	3973	307.34	10	0.910642401	0.009902366
Pyrimethamine	SLC47A1, SLC47A2, DHFR, STAT3	Tocris	4993	248.71	20	0.94083508	0.011272993
Neratinib	EGFR, ERBB2	haoyuan chemexpress	9915743	557.0427	2	0.870878319	0.014399249
AZD1152	AURKB	haoyuan chemexpress	9917232	507.6	20	0.89489027	0.017791455
KIN001-138	ROCK1	Nathanael Gray	NA	343.2	2.5	0.873707681	0.019398025
Geldanamycin	HSP90	haoyuan chemexpress	5288382	560.64	1	0.816578276	0.019946349
Paclitaxel	TUBB	haoyuan chemexpress	36314	853.9	0.1	0.836584602	0.020104874
Sorafenib	BRAF,ARAF,KIT,	LC Labs	216239	464.82495	2	0.886285282	0.020423825
GSK269962A	ROCK1	haoyuan chemexpress	16095342	343.2	2.5	0.763890925	0.022071023
CGP-082996	CDK4	haoyuan chemexpress	24825971	456.26	2	0.925287304	0.022377478
PD-173074	FGFR1	haoyuan chemexpress	1401	523.33	2	0.933527205	0.028942191
Parthenolide	NFKB	Tocris	5420805	248.3	10	0.862315424	0.034601722
XMD8-85	MAPK7	haoyuan chemexpress	46844147	459.54	5	1.014589081	0.035695586
Torin1	MTOR	Nathanael Gray	49836027	607.62	2.5	0.900751789	0.042365423
BMS-354825	ABL	haoyuan chemexpress	3062316	488	0.5	1.195456242	0.048009010
PHA665752	MET	Pfizer	10461815	641.61	1	0.905956965	0.066554097
A770041	SRC, LCK	haoyuan chemexpress	9549184	621.32	2	0.952191365	0.066567638
Roscovitine	CDK1	LC Labs	160355	354.45	15	1.031074143	0.073810427
SB203580	MAPK14	haoyuan chemexpress	176155	377.43	1	0.893150803	0.086759635
BMS-536924	IGF1R	haoyuan chemexpress	10390396	479.95	2	0.993413412	0.088425997
AZD-0530	SRC	haoyuan chemexpress	10302451	542.02	2	1.007490154	0.112067658
GNF-2	ABL	haoyuan chemexpress	5311510	374.1	2	1.017879095	0.123904066
Imatinib	ABL1,KIT,PDGFRB	haoyuan chemexpress	5291	493.6	2	0.940854931	0.166069753
PF-02341066	ALK,MET	haoyuan chemexpress	11496366	450.33	2	1.024313825	0.171490954
KIN001-135	IKBKE	haoyuan chemexpress	11626927	469.1	2.5	0.982153334	0.181712197
GO-6983	PKC	haoyuan chemexpress	3499	442.51	5	0.85665983	0.229269393
AMG706	KDR	haoyuan chemexpress	11667893	373.19	2	0.959940573	0.229307888

Supplementary table 2

Relative sensitivity of PDAC Cell Lines_ Fisher Exact Test Resu		Viability Threshold							
Cpd_Concentration	Publication_Name	0.1	0.2	0.3	0.4	0.5	0.6	0.7	0.8
1_High	Erlotinib	0.113476	0.383643	0.709858	0.104050	**0.026699**	**0.004725**	**0.002347**	**0.014709**
1_Low	Erlotinib	1.000000	1.000000	1.000000	1.000000	0.572868	0.701107	0.251509	**0.004441**
1_Med	Erlotinib	1.000000	1.000000	1.000000	0.616447	1.000000	**0.019523**	0.059591	**0.008140**
106_High	XMD8-85	1.000000	**0.035696**	0.299721	0.273921	0.430826	0.745982	1.000000	1.000000
106_Low	XMD8-85	1.000000	1.000000	1.000000	1.000000	1.000000	1.000000	1.000000	1.000000
106_Med	XMD8-85	1.000000	1.000000	1.000000	1.000000	1.000000	1.000000	1.000000	1.000000
11_High	Paclitaxel	**0.040628**	0.203638	0.329008	**0.033172**	0.473608	0.277983	0.094921	0.129876
11_Low	Paclitaxel	1.000000	1.000000	1.000000	1.000000	1.000000	1.000000	1.000000	0.383862
11_Med	Paclitaxel	1.000000	0.101007	0.215171	0.330451	0.863103	0.747807	0.327120	0.263205
110_High	Roscovitine	0.153700	0.736684	0.637968	0.474826	0.425349	0.178546	0.378021	0.502213
110_Low	Roscovitine	1.000000	1.000000	1.000000	1.000000	1.000000	1.000000	1.000000	0.146559
110_Med	Roscovitine	1.000000	1.000000	1.000000	1.000000	1.000000	1.000000	0.615044	0.090146
111_High	Salubrinal	0.529512	0.351026	0.069581	**0.001823**	**0.001182**	**0.000033**	**0.000550**	**0.047149**
111_Low	Salubrinal	1.000000	1.000000	1.000000	1.000000	1.000000	1.000000	0.091768	0.057560
111_Med	Salubrinal	1.000000	1.000000	1.000000	1.000000	1.000000	1.000000	0.183389	0.206575
119_High	Lapatinib	0.157210	0.102363	**0.029633**	**0.003865**	**0.035933**	**0.036176**	**0.018667**	**0.041403**
119_Low	Lapatinib	1.000000	1.000000	1.000000	1.000000	1.000000	0.393911	0.760076	0.822458
119_Med	Lapatinib	1.000000	1.000000	0.634595	0.157496	0.298193	0.089607	0.089282	0.233977
127_High	GSK269962A	0.144132	0.209252	0.270079	1.000000	0.419109	0.232843	**0.039373**	0.089430
127_Low	GSK269962A	1.000000	1.000000	1.000000	1.000000	1.000000	1.000000	1.000000	1.000000
127_Med	GSK269962A	1.000000	1.000000	1.000000	0.144132	0.429129	1.000000	1.000000	0.430686
14_High	Neratinib	0.632729	0.212874	**0.028169**	0.225148	0.338485	0.502695	0.174150	0.308054
14_Low	Neratinib	1.000000	1.000000	1.000000	1.000000	0.627546	0.248851	0.064780	1.000000
14_Med	Neratinib	1.000000	1.000000	0.252656	0.241206	0.102804	0.349263	0.501360	1.000000
17_High	Cyclopamine	1.000000	1.000000	1.000000	0.616447	0.390437	0.507025	0.821027	1.000000
17_Low	Cyclopamine	1.000000	1.000000	1.000000	1.000000	1.000000	1.000000	0.454367	**0.001856**
17_Med	Cyclopamine	1.000000	1.000000	1.000000	1.000000	1.000000	0.111255	0.118202	**0.002457**
18_High	SB203580	1.000000	1.000000	1.000000	1.000000	0.603177	0.610035	0.483589	0.147345
18_Low	SB203580	1.000000	1.000000	1.000000	1.000000	1.000000	1.000000	0.581115	1.000000
18_Med	SB203580	1.000000	1.000000	1.000000	1.000000	1.000000	1.000000	0.601413	0.228320
19_High	GO-6976	0.616238	0.158855	0.110404	0.090090	**0.004084**	0.100059	**0.024117**	**0.041717**
19_Low	GO-6976	1.000000	1.000000	1.000000	1.000000	1.000000	0.617391	1.000000	0.795782
19_Med	GO-6976	1.000000	1.000000	0.392421	0.101007	0.460902	0.231302	**0.012602**	**0.022909**
20_High	Geldanamycin	0.611965	0.099778	0.331388	0.141162	0.278280	0.381774	1.000000	0.236425
20_Low	Geldanamycin	1.000000	1.000000	1.000000	0.389936	0.250598	0.105276	0.299191	0.283913
20_Med	Geldanamycin	0.716642	0.149504	0.251009	**0.038772**	0.071118	0.146770	0.100999	**0.028242**
23_High	KN-93	1.000000	1.000000	0.183631	**0.014694**	0.063840	0.144275	0.374504	0.593422
23_Low	KN-93	1.000000	1.000000	1.000000	1.000000	1.000000	1.000000	1.000000	1.000000
23_Med	KN-93	1.000000	1.000000	1.000000	1.000000	1.000000	1.000000	1.000000	0.227807
29_High	AZ628	0.488219	0.702261	0.774515	0.497330	0.855776	0.138544	**0.003399**	**0.002510**
29_Low	AZ628	1.000000	1.000000	1.000000	1.000000	1.000000	1.000000	0.623480	0.755389
29_Med	AZ628	1.000000	1.000000	0.617485	1.000000	1.000000	0.415107	0.830754	0.357251
3_High	Rapamycin	1.000000	0.283516	0.726195	0.638511	0.587177	**0.037326**	0.084566	**0.022460**
3_Low	Rapamycin	1.000000	1.000000	1.000000	1.000000	0.572077	0.251009	0.257987	0.182650
3_Med	Rapamycin	1.000000	1.000000	0.111255	0.372137	0.419118	**0.035690**	**0.000999**	**0.003155**
30_High	Sorafenib	0.627944	0.260508	0.415144	0.346245	0.171015	0.214610	0.068166	**0.035530**
30_Low	Sorafenib	1.000000	1.000000	1.000000	1.000000	1.000000	1.000000	1.000000	1.000000
30_Med	Sorafenib	1.000000	1.000000	1.000000	1.000000	1.000000	1.000000	0.616333	0.715430
32_High	VX680	1.000000	0.547440	0.716865	0.439030	0.693183	0.737306	0.255809	0.170564
32_Low	VX680	1.000000	1.000000	1.000000	0.113949	**0.030004**	**0.016870**	0.052490	**0.000463**
32_Med	VX680	1.000000	1.000000	1.000000	0.411407	0.580823	0.197031	0.608897	0.873748
34_High	Imatinib	1.000000	1.000000	1.000000	1.000000	1.000000	0.261493	0.421461	0.733702
34_Low	Imatinib	1.000000	1.000000	1.000000	1.000000	1.000000	1.000000	1.000000	1.000000
34_Med	Imatinib	1.000000	1.000000	1.000000	1.000000	1.000000	1.000000	0.166070	1.000000
35_High	TAE684	1.000000	0.521806	0.108999	0.747962	1.000000	0.712550	0.497330	1.000000
35_Low	TAE684	1.000000	1.000000	1.000000	1.000000	1.000000	1.000000	1.000000	0.374202
35_Med	TAE684	1.000000	1.000000	0.305122	0.488219	1.000000	0.733702	0.439030	**0.007624**
36_High	PD-173074	1.000000	1.000000	0.166070	0.384968	1.000000	0.721030	0.416469	0.052203
36_Low	PD-173074	1.000000	1.000000	1.000000	1.000000	1.000000	1.000000	1.000000	0.174043
36_Med	PD-173074	1.000000	1.000000	1.000000	1.000000	1.000000	1.000000	1.000000	0.516763
37_High	PF-02341066	1.000000	1.000000	1.000000	0.389993	0.259990	0.564357	0.872560	0.376444
37_Low	PF-02341066	1.000000	1.000000	1.000000	1.000000	1.000000	1.000000	0.384968	0.175838
37_Med	PF-02341066	1.000000	1.000000	1.000000	1.000000	1.000000	1.000000	0.627944	0.346979
38_High	AZD-0530	1.000000	0.112068	0.433993	1.000000	0.377615	1.000000	0.745313	0.628995
38_Low	AZD-0530	1.000000	1.000000	1.000000	1.000000	1.000000	0.455837	1.000000	0.793241
38_Med	AZD-0530	1.000000	1.000000	1.000000	1.000000	1.000000	0.633223	0.574998	0.439940
4_High	LY294002	1.000000	1.000000	1.000000	1.000000	0.360918	0.150893	0.278731	**0.013249**
4_Low	LY294002	1.000000	1.000000	1.000000	1.000000	1.000000	1.000000	1.000000	0.610035

4_Med	LY294002	1.000000	1.000000	1.000000	1.000000	1.000000	1.000000	0.603177	0.794931
41_High	S-Trityl-L-cysteine	0.350600	**0.003148**	0.054976	**0.037083**	**0.007048**	**0.034115**	**0.020983**	0.271050
41_Low	S-Trityl-L-cysteine	1.000000	1.000000	1.000000	1.000000	1.000000	1.000000	1.000000	0.074772
41_Med	S-Trityl-L-cysteine	0.261493	0.384968	1.000000	1.000000	0.350277	**0.031584**	0.062007	**0.049804**
43_High	GO-6983	1.000000	1.000000	1.000000	1.000000	1.000000	1.000000	1.000000	0.358084
43_Low	GO-6983	1.000000	1.000000	1.000000	1.000000	1.000000	1.000000	1.000000	1.000000
43_Med	GO-6983	1.000000	1.000000	1.000000	1.000000	1.000000	1.000000	1.000000	1.000000
45_High	Z-LLNle-CHO / Z-LL-Norleucine-CHO	**0.002059**	0.382000	0.672347	0.789147	0.503905	1.000000	0.623480	1.000000
45_Low	Z-LLNle-CHO / Z-LL-Norleucine-CHO	1.000000	1.000000	1.000000	1.000000	1.000000	1.000000	1.000000	0.421461
45_Med	Z-LLNle-CHO / Z-LL-Norleucine-CHO	0.627944	0.161890	**0.040502**	0.419656	0.102730	**0.048093**	**0.013193**	0.348332
5_High	Sunitinib	0.151673	1.000000	0.611965	**0.018515**	**0.028242**	**0.005767**	**0.003796**	**0.005134**
5_Low	Sunitinib	1.000000	1.000000	1.000000	1.000000	1.000000	1.000000	1.000000	1.000000
5_Med	Sunitinib	1.000000	1.000000	1.000000	1.000000	1.000000	1.000000	1.000000	0.212642
51_High	BMS-354825	1.000000	0.072758	0.097948	0.085714	0.082331	0.165700	1.000000	1.000000
51_Low	BMS-354825	1.000000	1.000000	1.000000	0.232762	0.328364	1.000000	0.368262	0.239868
51_Med	BMS-354825	1.000000	0.550542	1.000000	0.769564	0.274416	0.116351	0.082227	0.083465
52_High	GNF-2	1.000000	1.000000	1.000000	1.000000	1.000000	1.000000	1.000000	1.000000
52_Low	GNF-2	1.000000	1.000000	1.000000	1.000000	1.000000	1.000000	1.000000	0.485939
52_Med	GNF-2	1.000000	1.000000	1.000000	1.000000	1.000000	0.123904	0.180097	0.485939
53_High	CGP-60474	**0.008021**	0.213742	0.227111	0.153035	0.579796	0.412291	0.232762	1.000000
53_Low	CGP-60474	1.000000	1.000000	1.000000	1.000000	1.000000	0.485939	0.223713	0.638185
53_Med	CGP-60474	0.485939	0.715150	0.113469	0.071020	**0.019675**	**0.002208**	**0.000443**	**0.042444**
54_High	CGP-082996	1.000000	1.000000	1.000000	1.000000	0.626089	0.162604	**0.048754**	0.319901
54_Low	CGP-082996	1.000000	1.000000	1.000000	1.000000	1.000000	1.000000	1.000000	0.232762
54_Med	CGP-082996	1.000000	1.000000	1.000000	1.000000	1.000000	1.000000	1.000000	0.519300
55_High	A770041	1.000000	1.000000	1.000000	0.415418	0.690257	0.617953	0.640690	0.320271
55_Low	A770041	1.000000	1.000000	1.000000	1.000000	1.000000	1.000000	1.000000	0.485939
55_Med	A770041	1.000000	1.000000	1.000000	1.000000	0.519300	1.000000	1.000000	0.130243
6_High	PHA665752	0.113476	0.165401	0.345003	0.517152	1.000000	0.714188	0.299698	0.123471
6_Low	PHA665752	1.000000	1.000000	1.000000	1.000000	1.000000	1.000000	1.000000	0.632887
6_Med	PHA665752	1.000000	1.000000	1.000000	1.000000	1.000000	1.000000	1.000000	0.351365
60_High	BI-2536	**0.008472**	**0.000569**	**0.000454**	**0.000008**	**0.000469**	**0.004069**	**0.006670**	1.000000
60_Low	BI-2536	1.000000	1.000000	1.000000	1.000000	0.521440	1.000000	1.000000	0.155399
60_Med	BI-2536	0.100736	**0.013668**	**0.002210**	**0.004076**	**0.002894**	**0.033846**	0.115352	0.051505
61_High	AMG706	1.000000	1.000000	1.000000	1.000000	1.000000	0.462712	1.000000	0.409622
61_Low	AMG706	1.000000	1.000000	1.000000	1.000000	1.000000	1.000000	1.000000	1.000000
61_Med	AMG706	1.000000	1.000000	1.000000	1.000000	1.000000	1.000000	1.000000	0.628878
62_High	BMS-536924	1.000000	1.000000	0.764143	0.523595	1.000000	0.209407	0.209692	0.219316
62_Low	BMS-536924	1.000000	1.000000	1.000000	1.000000	1.000000	1.000000	0.181082	0.088426
62_Med	BMS-536924	1.000000	1.000000	1.000000	1.000000	1.000000	1.000000	0.719328	0.182971
63_High	BMS-509744	1.000000	1.000000	1.000000	1.000000	1.000000	1.000000	0.158988	**0.002283**
63_Low	BMS-509744	1.000000	1.000000	1.000000	1.000000	1.000000	1.000000	1.000000	1.000000
63_Med	BMS-509744	1.000000	1.000000	1.000000	1.000000	1.000000	1.000000	1.000000	1.000000
64_High	cmk	1.000000	0.408381	0.064153	**0.010129**	**0.013905**	**0.000799**	**0.005356**	**0.042918**
64_Low	cmk	1.000000	1.000000	1.000000	1.000000	1.000000	1.000000	1.000000	1.000000
64_Med	cmk	1.000000	1.000000	1.000000	1.000000	1.000000	1.000000	1.000000	1.000000
65_High	JW-5-8-1	1.000000	0.286314	**0.036084**	**0.034723**	**0.004737**	0.119364	0.662704	0.131009
65_Low	JW-5-8-1	1.000000	1.000000	1.000000	1.000000	1.000000	1.000000	1.000000	1.000000
65_Med	JW-5-8-1	1.000000	1.000000	1.000000	1.000000	1.000000	0.791522	0.077380	**0.001182**
71_High	Pyrimethamine	**0.049155**	0.133842	0.798405	0.680051	0.111679	**0.022032**	0.271756	0.337115
71_Low	Pyrimethamine	1.000000	1.000000	1.000000	1.000000	1.000000	1.000000	1.000000	0.217450
71_Med	Pyrimethamine	1.000000	1.000000	1.000000	1.000000	0.642438	1.000000	0.608794	0.544465
83_High	Torin1	0.704781	0.525921	0.156795	**0.045150**	1.000000	1.000000	1.000000	1.000000
83_Low	Torin1	1.000000	1.000000	0.131132	0.680808	1.000000	0.589617	0.428549	0.267882
83_Med	Torin1	0.155567	0.588654	0.079830	0.464384	0.306567	0.272902	0.553054	1.000000
86_High	A-443654	0.269616	0.182870	**0.027193**	0.098069	0.473214	1.000000	0.713568	1.000000
86_Low	A-443654	1.000000	1.000000	1.000000	1.000000	1.000000	1.000000	1.000000	0.680808
86_Med	A-443654	0.632360	1.000000	0.460920	0.090941	**0.044079**	**0.010231**	**0.005913**	**0.027231**
87_High	GSK461364	**0.023640**	**0.002373**	**0.003587**	**0.019513**	0.074040	0.068041	0.474786	0.388578
87_Low	GSK461364	1.000000	1.000000	1.000000	1.000000	1.000000	1.000000	0.615886	0.105520
87_Med	GSK461364	**0.005431**	**0.001106**	**0.000610**	**0.021287**	**0.043696**	0.084007	0.215720	0.162785
88_High	MS-275	**0.014420**	**0.000991**	**0.003909**	0.068270	1.000000	1.000000	1.000000	1.000000
88_Low	MS-275	1.000000	1.000000	1.000000	1.000000	1.000000	1.000000	0.621791	0.566906
88_Med	MS-275	1.000000	0.389909	**0.042993**	**0.005230**	**0.000081**	**0.001271**	**0.013469**	**0.015561**
89_High	Parthenolide	**0.048320**	0.216530	0.443177	1.000000	1.000000	1.000000	0.762511	0.715235
89_Low	Parthenolide	1.000000	1.000000	1.000000	1.000000	1.000000	1.000000	0.609769	0.788165
89_Med	Parthenolide	1.000000	1.000000	0.283744	0.330198	0.275319	0.474786	1.000000	0.840986
9_High	MG-132	0.071118	0.190095	0.713849	0.833574	1.000000	1.000000	1.000000	0.617391
9_Low	MG-132	1.000000	1.000000	1.000000	1.000000	1.000000	0.519241	**0.033687**	**0.000606**
9_Med	MG-132	0.619753	0.503298	0.241513	0.299866	0.343193	0.283034	0.427258	0.723177

91_High	KIN001-135	1.000000	1.000000	1.000000	1.000000	1.000000	0.181712	0.522856	0.566265
91_Low	KIN001-135	1.000000	1.000000	1.000000	1.000000	1.000000	1.000000	1.000000	0.554180
91_Med	KIN001-135	1.000000	1.000000	1.000000	1.000000	1.000000	1.000000	0.234784	0.489386
93_High	KIN001-138	1.000000	0.619570	0.350674	**0.029679**	**0.047035**	0.053981	0.222255	0.429418
93_Low	KIN001-138	1.000000	1.000000	1.000000	1.000000	1.000000	1.000000	1.000000	0.616522
93_Med	KIN001-138	1.000000	1.000000	1.000000	1.000000	1.000000	0.616522	0.158754	0.339238
97_High	AZD6244	0.360469	0.109499	**0.020332**	**0.024615**	**0.007366**	**0.007957**	**0.020172**	**0.040149**
97_Low	AZD6244	1.000000	1.000000	1.000000	0.306330	**0.021208**	0.074775	**0.003263**	**0.003446**
97_Med	AZD6244	1.000000	0.770287	0.072480	0.070098	**0.000424**	**0.001188**	**0.007234**	**0.035881**
98_High	AZD1152	1.000000	0.100656	0.251828	0.364434	0.249842	0.263844	0.122659	0.512406
98_Low	AZD1152	1.000000	0.621835	0.506702	0.148235	0.108548	0.085558	0.080596	0.406424
98_Med	AZD1152	1.000000	1.000000	0.417698	0.128161	0.138183	0.139355	**0.025824**	0.071721

Appendix. Relevant Publications (2011-2014)

1: Alagesan B*, Contino G*, Guimaraes AR, Corcoran RB, Desphande V, Wojtkiewicz GR, Hezel AF, Wong KK, Loda M, Weissleder R, Benes CH, Engelman JA, Bardeesy N. Combined MEK and PI3K inhibition in a mouse model of pancreatic cancer. Clin Cancer Res. 2014 Oct 27. pii: clincanres.1591.2014. [Epub ahead of print] PubMed PMID: 25348516.

2: Tzatsos A, Paskaleva P, Ferrari F, Deshpande V, Stoykova S, Contino G, Wong KK, Lan F, Trojer P, Park PJ, Bardeesy N. KDM2B promotes pancreatic cancer via Polycomb-dependent and -independent transcriptional programs. J Clin Invest. 2013 Feb 1;123(2):727-39. doi: 10.1172/JCI64535. Epub 2013 Jan 16. PubMed PMID:23321669; PubMed Central PMCID: PMC3561797.

3: Hezel AF, Deshpande V, Zimmerman SM, Contino G, Alagesan B, O'Dell MR, Rivera LB, Harper J, Lonning S, Brekken RA, Bardeesy N. TGF-β and αvβ6 integrin act in a common pathway to suppress pancreatic cancer progression. Cancer Res. 2012 Sep 15;72(18):4840-5. doi: 10.1158/0008-5472.CAN-12-0634. Epub 2012 Jul 11. PubMedPMID: 22787119; PubMed Central PMCID: PMC3764481.

4: Yu M, Ting DT, Stott SL, Wittner BS, Ozsolak F, Paul S, Ciciliano JC, Smas ME, Winokur D, Gilman AJ, Ulman MJ, Xega K, Contino G,

Alagesan B, Brannigan BW,Milos PM, Ryan DP, Sequist LV, Bardeesy N, Ramaswamy S, Toner M, Maheswaran S, Haber DA. RNA sequencing of pancreatic circulating tumour cells implicates WNT signalling in metastasis. Nature. 2012 Jul 26;487(7408):510-3. doi:10.1038/nature11217. Erratum in: Nature. 2012 Oct 25;490(7421):570. PubMed PMID: 22763454; PubMed Central PMCID: PMC3408856.

5: Tzatsos A, Paskaleva P, Lymperi S, Contino G, Stoykova S, Chen Z, Wong KK, Bardeesy N. Lysine-specific demethylase 2B (KDM2B)-let-7-enhancer of zester homolog 2 (EZH2) pathway regulates cell cycle progression and senescence in primary cells. J Biol Chem. 2011 Sep 23;286(38):33061-9. doi: 0.1074/jbc.M111.257667. Epub 2011 Jul 11. PubMed PMID: 21757686; PubMed Central PMCID: PMC3190920.

6: Corcoran RB, Contino G, Deshpande V, Tzatsos A, Conrad C, Benes CH, Levy DE, Settleman J, Engelman JA, Bardeesy N. STAT3 plays a critical role in KRAS-induced pancreatic tumorigenesis. Cancer Res. 2011 Jul 15;71(14):5020-9. doi: 10.1158/0008-5472.CAN-11-0908. Epub 2011 May 17. PubMed PMID: 21586612; PubMed Central PMCID: PMC3693754.

7: Yang S, Wang X, Contino G, Liesa M, Sahin E, Ying H, Bause A, Li Y, Stommel JM, Dell'antonio G, Mautner J, Tonon G, Haigis M, Shirihai OS, Doglioni C, Bardeesy N, Kimmelman AC. Pancreatic cancers require autophagy for tumor growth. Genes Dev. 2011 Apr

1;25(7):717-29. doi: 10.1101/gad.2016111. Epub 2011 Mar 15. PubMed PMID: 21406549; PubMed Central PMCID: PMC3070934.

8: Ting DT, Lipson D, Paul S, Brannigan BW, Akhavanfard S, Coffman EJ, Contino G, Deshpande V, Iafrate AJ, Letovsky S, Rivera MN, Bardeesy N, Maheswaran S, Haber DA. Aberrant overexpression of satellite repeats in pancreatic and other epithelial cancers. Science. 2011 Feb 4;331(6017):593-6. doi: 10.1126/science.1200801. Epub 2011 Jan 13. PubMed PMID: 21233348; PubMed Central PMCID: PMC3701432.

Acknowledgements

I would like to express my gratitude to the director of the DIMET and tutor Prof. Andrea Biondi for his enduring support and admirable effort to promote clinician scientist training.